

ABSTRACT

Title of Document: DLC Thin Film Assisted ZnO Nanowires Growth

Sheng-Yu Young, Master of Science, 2008

Directed By:

Professor Lourdes Salamanca-Riba
Department of Materials Science and Engineering

In this study, we successfully fabricated dense, uniform, vertically aligned ZnO NWs on top of DLC films. The NWs' length, diameter and separation distance were controllable by fine tuning the growth parameters and changing the DLC film deposition temperature. HRTEM examination confirms the NWs were single crystalline with c-axis preferred orientation (lattice parameter $c = 0.519$ nm). From our experiment results, a ZnO polycrystalline layer forms first and then ZnO NWs grow on top of it. The NW has two sections. The bottom section has wider diameter of $100\text{nm} \sim 1 \mu\text{m}$, and the upper thinner section were about $20 \sim 80$ nm and it extends for $3 \sim 5 \mu\text{m}$ in length. EDS maps by SEM and TEM showed the elemental concentration of the Zn, O and C in NWs. From all the investigations, we established a model of growth mechanism for ZnO NWs growth on DLC film.

DLC THIN FILM ASSISTED ZINC OXIDE NANOWIRES GROWTH

By

Sheng-Yu Young

Thesis submitted to the Faculty of the Graduate School of the
University of Maryland, College Park, in partial fulfillment
of the requirements for the degree of
Master of Science
2008

Advisory Committee:

Professor Lourdes Salamanca-Riba, Chair / Advisor

Professor Mohamad Al-Sheikhly

Associate Professor Luz Martinez-Miranda

© Copyright by
Sheng-Yu Young
2008

Acknowledgements

First of all, I will give my highest appreciation to my advisor, Professor Lourdes Salamanca-Riba. Without her guidance, I couldn't achieve what I have now. Thanks for all her patience and kindness helping me get through the difficulties in school and life and giving me all the professional knowledge and research skill.

Second, I will have my special thanks to my colleague and group member Dr. Sung Hwan Lim. We are the best friends in school since day one. It's very pleasant to work with him and thanks for his precious help in the research. Hope we can work together again soon in the future. Thanks for Dr. R.D Vispute's research project that introduced me into this interesting ZnO NW research field.

Last but not least, I will give all my love to my lovely parents and the ones I love. They are the best. Love you guys so much! You are always the biggest support for me.

Table of Contents

Abstract	
Acknowledgements.....	ii
Table of Contents.....	iii
List of Tables.....	v
List of Figures.....	vi
Chapter 1. Introduction.....	1
1.1 Background.....	1
1.1.1 Motivation.....	1
1.1.2 One Dimension (1-D) Growth.....	3
1.2 ZnO properties and applications.....	5
1.3 Studies on ZnO Nanowires.....	6
Chapter 2. Sample Preparation and Experiments.....	12
2.1 Au, DLC Thin Films Deposition.....	12
2.1.1 Pulsed Laser Deposition (PLD).....	12
2.1.2 Films Deposition Parameters.....	14
2.2 ZnO NWs fabrication.....	14
2.2.1 Fabrication system.....	14
2.2.2 ZnO NWs Growth Conditions.....	16
2.3 Characterization techniques.....	18
2.3.1 Scanning Electron Microscopy (SEM).....	18
2.3.2 Atomic Force Microscopy (AFM).....	20
2.3.3 Photoluminescence (PL).....	21
2.3.4 X-ray Diffraction (XRD)	22
2.3.5 Transmission electron microscopy (TEM).....	23
Chapter 3. Results and Discussion.....	25
3.1 Au Thin Film assisted ZnO NWs Growth.....	26
3.1.1 Growth Parameters.....	26
3.1.2 Temperature Dependence.....	26
3.1.3 Zn Weight Dependence.....	28
3.1.4 Gas flow Dependence.....	29
3.1.5 Au Thin Film Thickness dependence.....	29
3.1.6 Optimized Growth Condition.....	31
3.2 DLC Thin Film assisted ZnO NWs Growth.....	34
3.2.1 DLC Film Deposition Temperature Dependence.....	35
3.2.2 DLC Film Thickness Dependence.....	39
3.2.3 ZnO NWs Growth Dependence on Temperature.....	42
3.2.4 Oxygen partial pressure dependence.....	43
3.3 Chemical, Structural and Optical characterization of ZnO NWs Grown on DLC film.....	46
3.3.1 Scanning Electron Microscopy (SEM).....	46

3.3.2 Atomic Force Microscopy (AFM)	48
3.3.3 X-ray Diffraction (XRD).....	50
3.3.4 Photoluminescence (PL).....	52
3.3.5 Transmission electron microscopy (TEM).....	53
3.4 ZnO NWs Growth Mechanism.....	58
Chapter 4. Summary and Suggestions for Future Work.....	64
4.1 Summary.....	64
4.2 Suggestions for Future Work.....	65
References.....	67

List of Tables

Table 3.1	Growth dependence on the Ar/O ₂ flow (sccm) and oxygen partial pressure (P_{O_2} %). In our growth system, Ar/O ₂ of 20/1 (P_{O_2} = 4.76%) and 20/2 (P_{O_2} =9.06%) show the most uniform and well-aligned ZnO NWs.....	44
-----------	--	----

List of Figures

Figure 1.1	Figure 1.1 (A~F) Schematic illustrations of 6 different strategies that have been demonstrated for achieving one dimensional growth.....	4
Figure 1.2	The Au metal tip on top of a nanowire when a thin Au layer or a nanosized Au particle is used as nucleation site. The NW growth will grow underneath the Au particle and the Au particle remains on the tip of the nanowire.....	9
Figure 1.3	(a) DLC is known has low work function for field emission. When the NWs grow on the DLC film, the Fermi level is lifted up and the work function lowered for the ZnO NW/DLC film combination. (b) When the NWs grown on DLC film have a better vertical growth alignment and better crystalline structure the β value in Fowler-Nordheim equation is reduced. This constant is usually used to determine the field emission enhancement factor.....	10
Figure 2.1	Schematic of pulsed laser deposition (PLD) system. Au and graphite target was placed on the target holder for Au and DLC thin film deposition. The heatable stage allows us to deposit the DLC film at different temperature. The DLC thickness gradient was controlled by an automatic, speed-controlled metal shield in front of the substrate.....	13
Figure 2.2	The schematic of thermal evaporation system for fabricating ZnO NWs, in which a quartz tube of 2.5 cm in diameter lies in a horizontal	

tube furnace. The inset red line represents the actual temperature gradient (at 900 °C programmed temperature) within the furnace measured by the inserted thermocouple. The source material (Zn powder only) was loaded in a ceramic boat situated at the left side (upstream) of the tube. The substrates on the holder were located at the right side of the tube (downstream). The schematic represents the optimized location of both boats in our fabrication system.....16

Figure 2.3 The interdependence relations between variables. The main variables are catalyst thickness, substrate, Zn powder heating temperature, gas carrier flow rate, and oxygen partial pressure. All the variables are closely related to each other and can make huge difference in results such as the length, density, diameter and the alignment of the ZnO NWs.....18

Figure 3.1 (a) ~ (d) ESEM (ESEM stage 45° tilted) sample images show the ZnO NWs growth results at various substrate temperatures (from 500 ~ 800 °C). The ZnO NW growth temperature is the only variable here. We can see the trend of the NWs' diameter is decreased when the substrates temperature was increased. The diameters decreased from μm range to tens of nm range. The inset in (d) is a magnified FESEM image of the NWs. The uniformity of the ZnO NWs is also getting better when we increase the NW growth temperature.....27

Figure 3.2 (a) ~ (d) FESEM images for varying Zn powder weight from 3g to 0.2g. Image (a) is covered by dense tetrapod shape ZnO added-on by

deposition on top of the substrate surface. Images (b) and (c) have less and less unwanted deposition on top of the ZnO NWs. (d) When the Zn weight reduces to near 0.25 ~ 0.2g, nanowires with uniform diameter, and vertically oriented grow on the substrate surface...27

Figure 3.3 When the substrate is heated in the fabrication system, the nanometer thick Au film melts and turns into nanosized Au particles that act as nucleation sites for the growth of the nanowires.....30

Figure 3.4 Schematic (bottom) of Au catalyst layer with gradient in thickness and its dependence on the ZnO NWs growth. SEM image (a) is the NWs with thinner (0~10 nm) Au layer area where the ZnO NWs grow vertically and uniformly. Image (b) represents the morphology of the growth at the thicker (> 15 nm) area where the ZnO has various shapes and diameter.....31

Figure 3.5 SEM images taken from nanowires grown with optimized parameters but different predeposited Au layer thickness on Si (001) substrate. Images (a), (b) are for 5 nm thick Au layer and images (c), (d) are for 1 nm thick Au film. The nanowires' length increases from ~200 nm in (a), (b) to > 1000 nm in (c), (d).....33

Figure 3.6 Schematic and SEM image of the ZnO NWs selective growth with 1nm and 10nm Au thin film. The ZnO NWs grown on 1nm thick Au layer shown in area (i) in the SEM image. The NWs in this area are well-aligned and uniform. The growth in area (ii) is much more

	random and there is no preferred orientation. The bare SiO ₂ area is very clean with almost no nanowire growth.....	34
Figure 3.7	(a) Schematic of the DLC thin film pattern predeposited on SiO ₂ /Si (001) substrate before nanowire growth. Images (b) to (d) are the ZnO NWs growth morphology on DLC films that were deposited at room temperature (b), 400 °C (c) and 600 °C (d). The NWs length decreases when the DLC deposition temperature increases.....	37
Figure 3.8	SEM images of NWs grown on DLC film deposited at R.T. (a, b), 200 °C (c, d) and 400 °C (e, f). Other ZnO NWs growth parameters were the same for all three samples. From the magnified SEM images (b), (d) and (f), we can see the ZnO grain underneath the nanowires. The grain size decreases when the deposition temperature (in at the range of R.T to 400 °C) of the DLC film increases. The smaller grain size results in higher nanowire density.....	38
Figure 3.9	SEM image of ZnO NWs selective growth on DLC film pattern and schematics of 100 μm × 100 μm size DLC pad pattern and a thickness gradient in the range of 1 ~ 100 nm along a 10 mm long Si substrate. The selective area growth shows the NWs preferred to grow on DLC film but not on SiO ₂ surface.....	37
Figure 3.10	(a) ~ (d) are the SEM images of the ZnO NWs morphologies grown on different thickness (1~100nm) of DLC film of the substrate. The schematics show the changes of NW/NR length and diameters grown on different DLC thickness. The plot shows the trend of the diameter	

and the length of ZnO NW/NR with the DLC film thickness and the inset is the ZnO NW/NR uniformity trend. The uniformity is better when the NWs grow on the thinner ($< 20\text{nm}$) and thicker ($> 75\text{nm}$) DLC film. Note that, for this set of samples the only variable is the DLC film thickness. A change of any of the other growth parameters will have different result.....41

Figure 3.11 SEM images of the nanowire/nanorods morphology on the region of DLC thickness $t_{\text{DLC}} = 1 \sim 15 \text{ nm}$. (a ~ c) are normal view images and (d) has a 50° sample tilt. Image (c) shows the porous morphology underneath the NRs and the NWs/NRs are faceted indicating high degree of crystallinity.....42

Figure 3.12 (a) – (c) shows the growth temperature dependence on the NW morphology. The growth temperature was set to 850, 900, and 1000 °C, respectively. It reveals the same trend as for Au film assisted growth which the NWs density and diameter decreases when the growth temperature increases.....43

Figure 3.13 SEM images showing NWs grown on DLC film with the optimum parameters to obtain high density ($17 \text{ NM} / \mu\text{m}^2$), thin ($20 \text{ nm} \sim 80 \text{ nm}$) and long ($4 \mu\text{m}$ for 30 mins growth) NWs with uniform distribution.....45

Figure 3.14 Different ZnO NWs morphologies observed in this study. There is a ZnO polycrystalline film that forms at the first stage of the growth and the NWs grow on top of it. ZnO NWs have two sections. The bottom

section (nanorod) has wider diameter varying from 100 nm up to 1 μm , depending on the growth conditions. The thinner section on top uniformly grows down to ~ 20 nm in diameter and has a *c*-axis orientation along the growth direction. The NWs extend for 3 \sim 5 μm in length.....47

Figure 3.15 SEM image and EDS line scan. (a) is the SEM image of scanned area. The spectrum in (b) shows strong peaks of Zn, O and C (from the DLC film). The EDS line scan (c) reveals the ZnO NW is uniform with Zn and O exhibiting the same trend and C remains fairly constant and low. Image (d) is the 3 μm long single NW chosen to be examined for 3 mins from bottom to top.....48

Figure 3.16 (a) is the schematic (vertical and side view) of Si (001) with 30 nm DLC pattern on top deposited at room temperature. (b) shows the SEM images after growth of ZnO NWs. AFM image (c) is the as deposited DLC film topography prior to NWs growth and (d) is the sample surface examined after etching in 5% HCl solution for 24 hours revealing the rough surface of the DLC after growth.....50

Figure 3.17 Comparison of X-ray Diffraction (XRD) spectra from bare SiO₂/Si substrate, DLC/SiO₂/Si, ZnO NWs/DLC/SiO₂/Si growth and after etching the NWs in diluted HCl solution for 24 hours. After etching (spectrum (4)), the ZnO NW (002) peak disappeared.....51

Figure 3.18 Photoluminescence (PL) spectra of ZnO NWs grown on DLC film (DLC/SiO₂/Si) and on Au film (Au/SiO₂/Si). The strong ultraviolet

	emission at around 380 nm is attributed to the near-band-edge emission of the wide bandgap ZnO.....	53
Figure 3.19	(a) and (b) are cross-section and top view SEM images of the ZnO NWs grown at optimum conditions for high density, thinner diameter and straight NWs on DLC film. The diameter of the NWs ranges from 20 to 80 nm. (c) is the cross-section view TEM image and (d), (e) are the high-resolution TEM images. (e) shows the nanostructure on the top part of the NW.....	55
Figure 3.20	TEM image showing the area and directions along which EDS line scans were obtained. Horizontal line scan (H, red dash arrow) shows uniform composition and vertical line scan (V, blue dash arrow) shows the quantitative information of the concentration of each element. From the chart, we can see the ZnO NW is oxygen deficient. This results in the ZnO being an intrinsic n-type semiconductor.....	56
Figure 3.21	TEM image (a) shows the selected area for EDS mapping. Note that the M-bond still exists over the NWs since the ion-milling time for TEM sample preparation was short. The EDS maps in (b) are for O, Zn, C and Si.....	57
Figure 3.22	TEM images and EDS maps from a single ZnO NWs area. The elemental maps show the NW is pure ZnO and there is no C content within it.....	58
Figure 3.23	(a) Schematic of the evaporation chemical vapor, transport and condensation during fabrication process. Zn vapor evaporates from the	

Zn metal powder from higher temperature zone located upstream and transported by the carrier gas (Ar/O₂) to the surface of DLC film and react. (b) Vertical view schematic of the DLC film surface. The arrows show the movements of ZnO impel by the driving force resulting from its immiscibility with C on the surface. It also shows the possible reactions between ZnO and C at the DLC surface and the morphology of the ZnO NWs.....63

Chapter 1

Introduction

1.1 Background

The synthesis of semiconductor nanomaterials has attracted great attention in the last few years. Due to their large surface area to volume ratios, size effects and possible quantum confinement effects, nanomaterials are predicted to exhibit outstanding and enhanced properties compared to those of bulk materials and also offer routes to fabricating novel nanodevices [1]. One-dimensional (1-D) nanostructures, such as nanowires and nanotubes, represent the smallest dimension for efficient transport of electrons and excitons. They have the ideal morphology and dimension for functional nanoscale electronic and photonic structures and have been regarded as the most promising building blocks for nanoscale electronic and optoelectronic devices.

1.1.1 Motivation

Ever since the discovery of carbon nanotubes by Iijima [2], the synthesis of tubular nanomaterials has aroused worldwide interest --- both in fundamental studies, and for their potential applications. For example, wurtzite structured zinc oxide (ZnO) is dragging a significant attraction in research due to its wide direct band gap (3.37

eV) at room temperature and a high exciton binding energy of 60 meV [3] and is recognized as a potentially important optoelectronic material, and has already been used to fabricate demonstrator light-emitting devices (LEDs), transparent electronics and many optoelectronic devices [4-8]. The studies for 1-D ZnO nanowires are focused on their electronic, optical, mechanical properties and their versatile applications, such as optoelectronics, photovoltaics and sensors. Therefore, optimizing the ZnO NWs' fabrication process, understanding their fundamental properties and growth mechanism and developing techniques to fabricate novel NWs devices are all equally important.

In recent years, researchers fabricate ZnO nanowires on pre-deposited catalytic thin film layers or nano-particles to improve the growth conditions, such as Au film/particle or ZnO pre-coated thin film. However, metal pre-deposited layers or particles usually have metallic tips on top of ZnO nanowires which may change the properties and restrict the potential applications.

In this study, we first tried to find the growth condition through commonly used Au thin film to assist ZnO NWs growth and then replace the Au layer with diamond-like carbon (DLC) layer playing a similar role as Au assisting the nanowires growth for selective growth but avoiding the drawback of having a metal particle on of the nanowires' tips. Moreover, the architecture of ZnO NWs/DLC film opened up a new regime of application possibilities when the DLC film was introduced, since DLC film can be deposited at room temperature. Thus the process is low cost and DLC almost can attach to any surface. Another reason we choose the DLC film is to take advantage of its sp^2/sp^3 bonding content to understand the growth mechanism through

the reactions between carbon and ZnO, since most of the research of fabricating ZnO NWs use a mixture of ZnO powder and graphite powder. At certain temperature (usually the process of $ZnO + C_{(graphite)} \xrightleftharpoons{>970^{\circ}C} Zn + CO$ can only take place when the fabrication temperature is higher than 970 °C according to Ellingham Diagram), the carbon will participate in a redox reaction during the growth process. Although the theoretical suggestions for the chemical reactions around the substrate and the ZnO NWs growth mechanism are very likely to take place; there is still no direct proof to demonstrate those suggestions. We expect that the DLC film may offer direct observation for the carbonic reactions and help explain the ZnO NWs growth mechanism.

1.1.2 One-dimensional (1-D) growth

It is generally accepted that one dimension nanostructures provide a good system to investigate the dependence of electrical and thermal transport, and mechanical properties on dimensionality and size reduction (or quantum confinement). They are also expected to play an important role as both interconnections and functional units in fabricating electronic, optoelectronic, electrochemical, and electromechanical devices with their nanoscale dimensions. 1-D nanostructures can now be fabricated using a number of advanced nanolithographic techniques, such as electron-beam (e-beam) or focused-ion-beam (FIB) writing, proximal-probe patterning, and X-ray or extreme-UV lithography. Further development for these techniques is needed for higher through-put, lower cost, more diverse-ranged materials, larger quantities, etc.

Other 1-D nanostructure growth techniques are also developing in parallel. Some of these methods are based on chemical synthesis and can provide an alternative approach for generating 1-D nanostructures in terms of material diversity, cost, and the potential for high volume production. In the past few years, chemical methods have been demonstrated as the “bottom-up” approach for fabricating 1-D nanostructures with various controls over the parameters. Figure 1.1 schematically illustrates some of the synthetic strategies including [9]: (I) Intrinsic anisotropic crystallographic structure of a solid to accomplish 1-D growth; (1A); (II) Introducing a liquid-solid interface to reduce the symmetry of a seed; (1B); which is the main approach we are using in this thesis study; (III) Use of templates with 1-D morphologies to direct the formation of 1-D nanostructures; (1C); (IV) Supersaturation control to modify the growth; (1D); (V) Kinetic control of the growth rate of various facets of a seed; (1E); (VI) Self-assembly of 0D nanostructures; (1F); (VII) Size reduction of 1-D microstructures (not shown).

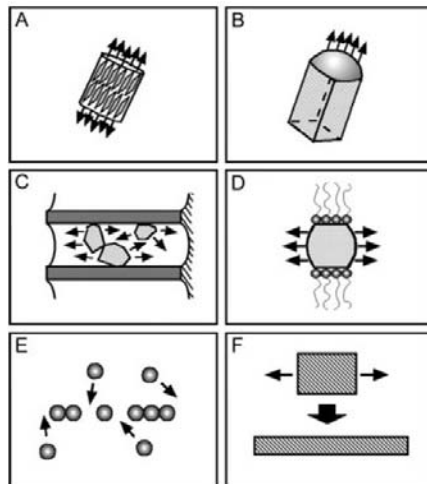


Figure 1.1 (A~F) Schematic illustrations of 6 different strategies that have been demonstrated for achieving one dimensional growth [9]

1.2 ZnO properties and applications

As semiconductor devices become smaller and smaller, the dimensions of new electronic components are reaching nanometer scale. Understanding the fundamental properties of these new devices and component materials, such as their electronic structures and band gaps, provides opportunities to apply advanced materials to fabricate new devices for future applications.

In semiconductors, when electrons fall from the conduction band to the valence band, they emit light. This effect is commercially exploited for devices such as light-emitting diodes (LEDs) and semiconductor lasers. ZnO is a n-type, direct wide band gap semiconductor ($E_g \sim 3.37\text{eV}$ at room temperature), which is suitable for production of light emitting devices with lasing action in the visible range of green, blue, ultraviolet, or white light. Its high exciton binding energy (60 meV) is much larger than the materials commonly used for blue-green light emitting devices, such as GaN (~ 25 meV) and ZnSe (~ 22 meV), and is expected to have efficient excitonic laser action at room temperature. This indicates that the excitons in ZnO are thermally stable at room temperature.

In addition, ZnO has also been investigated as a short-wavelength light emitter, a transparent conductor and piezoelectric material. The conductance of ZnO NWs is extremely sensitive to exposure to ultraviolet (UV) light. The light-induced insulator-to-conductor transition enables ZnO NWs to reversibly switch between OFF and ON states [10].

With these outstanding properties, ZnO is a promising candidate for applications like UV laser diodes, blue-green optoelectronic devices, light-emitting diodes (LEDs), gas or chemical sensors, transparent electrodes, cold cathode and also applications in solar cells. ZnO doped with magnetic elements is also a promising candidate for spintronics that would corroborate theoretical predictions of room temperature ferromagnetism [11]. In addition, the non-centrosymmetric crystallographic structure and spontaneous surface polarization characteristics make ZnO one of the most exciting oxide nanostructures for investigating nanoscale physical and chemical phenomena [12].

1.3 Studies on ZnO NWs

ZnO nanostructures with different morphologies like nanowires [13], nanobelts [14], nanorings [15], nanobridges and nanocombs [16] have been grown and explored using various methods, such as metal–organic chemical vapor deposition (MOCVD) [13], pulsed laser deposition (PLD) [14], and chemical vapor deposition (CVD) [15]. However, most reports present studies of ZnO nanostructures that are synthesized by conventional thermal evaporation process or thermal chemical vapor transport condensation system [15-17]. The various morphologies of ZnO nanostructures should have distinctive applications. For example, the nanobelts could be used as field effect transistors [18], ultra-sensitive gas sensors [19], nanoresonators [20] and nanocantilevers [21].

ZnO nanowires with good alignment on the substrate are of particular importance for their potential applications in the fabrication of devices. The

controlled growth of vertically aligned ZnO nanowires/nanorods has been demonstrated on substrates with metal nanoparticles (or thin film) as catalysts [22-23] or on substrates with good lattice matching such as sapphire substrate or ZnO thin layer pre-coated Si substrates [24-33]. ZnO NWs also can directly deposit on other 1-D nanostructures such as GaN, GaP, SiC nanowires or carbon nanotubes (CNTs) [34-35].

New synthesis methods are fast developing for the growth of ZnO NWs. These methods are expected to be more feasible for the highly demanding devices and make this material more promising for practical usage in the near future. ZnO powder mixed with 20 ~ 50 wt% of graphite powder is commonly used as the materials resource in fabrication. Although the mechanism of how the mixture contributes to the growth is not clear; it's been widely accepted that the graphite powder mixed in ZnO powder can improve the growth condition.

In this study, we investigated the growth mechanism of ZnO NWs assisted by diamond-like carbon (DLC) thin film, instead of metal thin film or nanoparticles, to avoid the metal particle from diffusing to the top of the nanowires and also to provide selective nucleation sites for nanowires growth.

Why DLC thin film layer is used to improve the ZnO NWs growth? First of all, in ZnO NWs growth research, most of the common source material is a mixture of graphite powder with ZnO powder. In this study, we pre-deposited a diamond-like carbon (DLC) film on the Si substrate. It's known that the DLC film is a combination of sp^2/sp^3 bonding. We expect the graphite sp^2 bonding portion can provide direct carbon content during fabrication and assist the NWs growth. Even though the role

of carbon in the growth process is still not well understood (most researchers suggest that a redox process is usually undertaken during the growth process); however, it is known that the presence of carbon indeed improves the ZnO NWs growth. The crystalline graphite with sp^2 bonding, and amorphous carbon with sp^2 and sp^3 bonding, of the DLC film are well studied. It is known that the sp^2/sp^3 bonding will vary with DLC deposition temperature [36]. It's usually true that the sp^2/sp^3 ratios increase with decreasing substrate temperature during depositing DLC film utilizing plasma related deposition technique such as pulsed laser deposition (PLD), chemical vapor deposition (CVD) or physical vapor deposition (PVD) [37, 38]. Therefore, the graphite portion in DLC thin film may have the possibility to play a roll as the carbon source to the ZnO NWs growth process. From this unique source of carbon during the fabrication, we can study the role of carbon content in the ZnO NW fabrication process. In addition, the DLC film provides selective area growth nucleation site. Therefore, we can use no metal catalyst for nucleation and there will be no metal (Au) tip on top of the NWs (Figure 1.2).

Second, for application purposes, DLC thin film is high in mechanical hardness and is a semiconductor with a varied band gap (from 1 eV to 5eV depending on the density of the sp^2/sp^3 bonding type; 5.5eV for diamond). It is also chemically inert and optically transparent which is good for optical applications [36].

Moreover, there is a great interest in nano-structured carbon films for the potential use as cathodes in field emission displays (FEDs); plus, the DLC thin film is low-cost since it can be fabricated at room temperature by various plasma deposition techniques. It's known that the work function of DLC thin film ($\Phi_{DLC\ film}$) is also low

which can reduce the ZnO NWs' power consumption in practical applications from lowering the combined work function ($\Phi_{combination}$).



Figure 1.2 The Au metal tip on top of a nanowire when a thin Au layer or a nanosized Au particle is used as nucleation site. The NW growth will grow underneath the Au particle and the Au particle remains on the tip of the nanowire.

In Y.H. Yang et al.'s research [39], they showed a remarkable enhancement of the field emission intensity of the ZnO nanowires covered by amorphous diamond compared to that of the intrinsic amorphous diamond. Decorating an amorphous diamond layer with one-dimensional nanostructures on its surface could largely improve the field emission property. The Fowler-Nordheim (F-N) equation/plot is usually used in the study of field emission property of a material. The F-N plots were used to determine the turn-on (threshold) voltage (V), work function (Φ), field enhancement coefficients (β) and effective emission areas. The relations between the relevant work functions of ZnO and DLC are shown in **Figure 1.3 (a)**.

Fowler-Nordheim Equation:

$$J = A \frac{(\beta F)^2}{\Phi} \exp\left(\frac{B\Phi^{3/2}}{\beta F}\right),$$

where

J : the current density

Φ : the barrier height (eV), work function

F : applied field

β : a dimensionless geometric
field emission enhancement factor

βF : the local field at emission site

A, B : constants

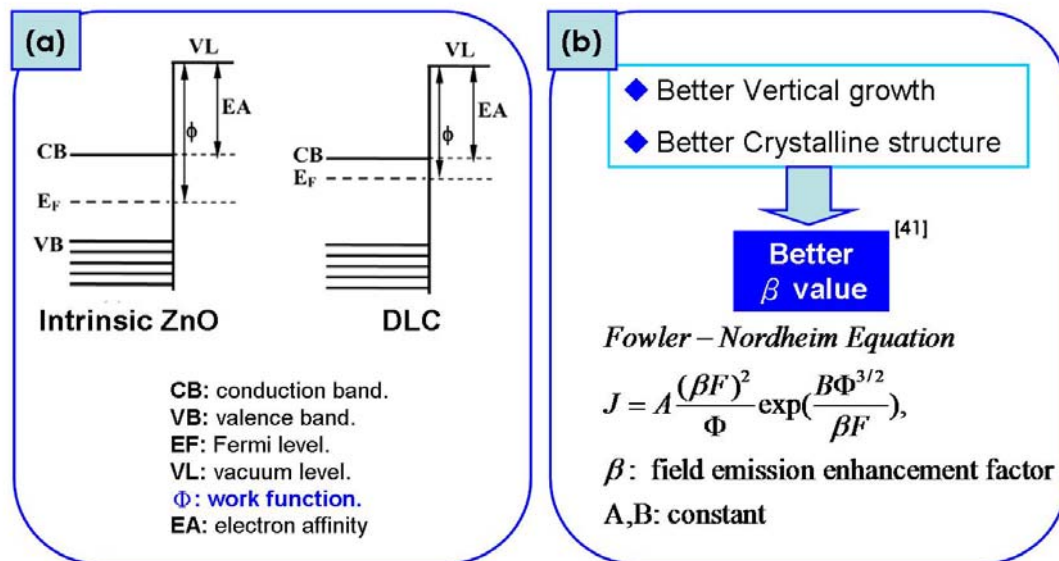


Figure 1.3 (a) DLC is known has low work function for field emission. When the NWs grow on the DLC film, the Fermi level is lifted up and the work function lowered for the ZnO NW/DLC film combination. (b) When the NWs grown on DLC film have a better vertical growth alignment and better crystalline structure the β value in Fowler-Nordheim equation is reduced. This constant is usually used to determine the field emission enhancement factor.

It is impossible to independently determine two parameters: the field emission enhancement coefficient and the work function from the F-N plot alone. The field

enhancement coefficients are calculated from the geometry of the emitting system. The effective work function for different DLC film coatings are normally determined from the slope of the F-N plots using the calculated β coefficient.

Based on the F-N plot of ZnO NWs deposited on amorphous diamond samples in Yang et al.'s research [40], the data fit to a linear relationship. From their calculation, the work function of the DLC film is 1 eV (3 ~ 5nm thick DLC film). The β -value (field emission enhancement factor) of DLC film alone was calculated to be 76. As for the DLC film deposited with ZnO NWs on top, the β -value can reach 900 using the ZnO work function of 5.3 eV [41, 42]. Yang also demonstrated that the layer of ZnO NWs covering the DLC film can significantly improve the field emission property compared to DLC film alone [40]. However, the ZnO NWs in their research were poorly grown and were not well aligned.

It's known that the β -value varies with the geometry, structure, tip size, and density of ZnO NWs. Tseng et al. also pointed out that better vertical growth, better crystalline structure and lower density of ZnO NWs can lead to higher β -value [42] (**Figure 1.3 (b)**). Therefore, from all the information above, DLC thin film layer is not only another carbon source material that assists in the growth of ZnO NWs, but also itself has many remarkable electronic and optical properties that could make the fabrication of ZnO NWs devices possible.

In this thesis, chapter 2 describes the details of the experimental techniques used in this work. Chapter 3 shows the results of the growth results and a discussion of the results with the relation between growth conditions and properties. Finally, chapter 4 presents a summary of the work and suggestions for the future work.

Chapter 2

Sample Preparation

2.1 Au, DLC Thin Film Deposition

Nanostructured materials have attracted great attention because of their unique physical properties and significant applications. One-dimensional (1-D) nanostructures, such as nanowires and nanotubes, represent the smallest dimension for efficient transport of electrons and excitons. They have the ideal morphology and dimension for functional nanoscale electronic and photonic structures and have been regarded as the most promising building blocks for nanoscale electronic and optoelectronic devices.

2.1.1 Pulsed Laser Deposition (PLD) system

Prior to ZnO deposition, thin Au or DLC film layer was deposited by pulsed laser deposition (PLD). The deposited thin films provide selective growth and improve the deposition conditions by providing the ZnO nanowires nucleation sites to grow. **Figure 2.1**, shows the simple schematic of the PLD system, it includes a KrF excimer laser source, and optical system with an aperture, a mirror, and focusing lens. The round shape chamber is equipped with a substrate heater, heating stage, rotating target holder and a vacuum system.

For the Au and DLC thin film deposition in this study, a KrF excimer laser with a 248 nm wavelength and 30 ns pulse width was used. During the deposition process, the pulsed laser beam is focused onto a target to increase the laser energy density (energy/unit area at target surface) by a focusing lens. The focused laser beam which has higher energy than the threshold value dissociates and ablates the target material and forms a plasma plume. The plume is normal to the target surface and deposits the expected materials on the substrate.

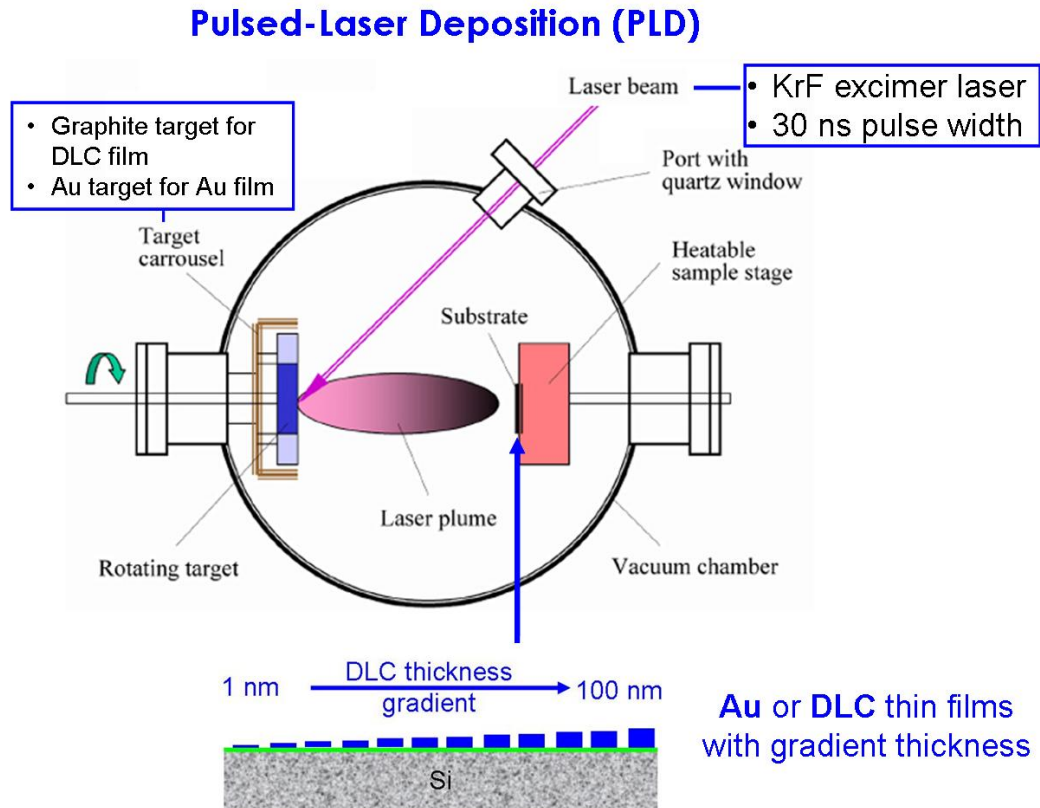


Figure 2.1 Schematic of pulsed laser deposition (PLD) system. Au and graphite target was placed on the target holder for Au and DLC thin film deposition. The heatable stage allows us to deposit the DLC film at different temperature. The DLC thickness gradient was controlled by an automatic, speed-controlled metal shield in front of the substrate.

2.1.2 Film Deposition Parameters

Au or graphite target was placed on the target holder for Au and DLC thin film deposition. The heatable stage allows us to deposit the DLC film at different temperatures. The DLC thickness gradient was controlled by an automatic, speed-controlled metal shield in front of the substrate. A laser energy of 680 mJ at a frequency of 10 Hz was used for PLD deposition for both Au and DLC thin films. For Au deposition, the chamber was pumped first to $\sim 5 \times 10^{-6}$ Torr and a Au film was deposited from a Au target at room temperature. The Au film thickness was varied from 1 ~ 100 nm for optimizing the growth conditions. The DLC films were deposited from a graphite target at various temperature ranging from 200 ~ 600 °C and the thickness was also varied from 30 ~ 100 nm to investigate the thickness dependence of growth conditions. A DLC film with a thickness gradient was deposited on a substrate for fast parameter optimization.

2.2 ZnO Nanowire Fabrications

2.2.1 Fabrication System

A thermal evaporation system, also called *vapor transport and condensation process (VTCP)* or *chemical vapor transport condensation (CVTC)*, in which a quartz tube of 2.5 cm in diameter lies in a horizontal tube furnace without a vacuum system was used to fabricate ZnO NWs. The experimental setup and the temperature gradient

within the furnace are shown in [Figure 2.2](#). The temperature gradient in the furnace was very important in determining the optimum deposition temperature for ZnO NWs.

Zn powder of 99.99% purity was used as the ZnO source material. The substrates were (100) oriented Si wafers with a pre-deposited thin Au or diamond-like carbon (DLC) layer with a thickness of 10 ~ 50nm utilizing pulsed laser deposition (PLD) technique. For the Au film, the deposition temperature was always at room temperature. However, in order to investigate how the ZnO NWs growth condition changes with the variation of DLC films' deposition condition, we deposited DLC films using PLD (Figure 2.1) at different substrate temperatures (room temperature, 200 °C, 400 °C and 600 °C) at a deposition pressure of $\sim 4 \times 10^{-5}$ Torr. The programmed temperature for ZnO NW growth in our thermal evaporation system was varied from 500 °C to 1150 °C to investigate the optimum growth temperature. Zinc powder (from 3 g down to 0.2 g) was used and placed in a ceramic boat located at the left side center of the tube and the Au or DLC patterned Si substrates were situated near the right end of the furnace. A mixture of Ar/O₂ gas mixture is used as carrier gas with controlled flow rate and ratio. The optimum flow rate in our deposition system was about 22 sccm.

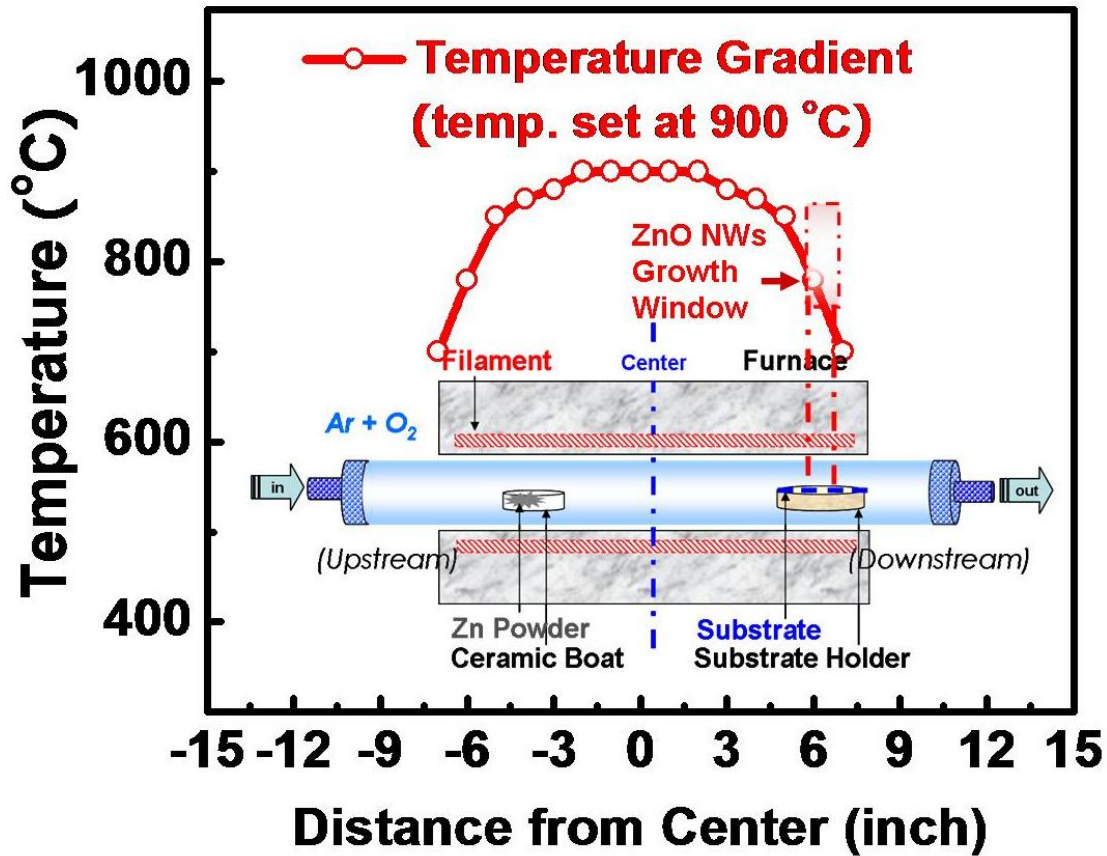


Figure 2.2 The schematic of thermal evaporation system for fabricating ZnO NWs, in which a quartz tube of 2.5 cm in diameter lies in a horizontal tube furnace. The inset red line represents the actual temperature gradient (at 900 °C programmed temperature) within the furnace measured by the inserted thermocouple. The source material (Zn powder only) was loaded in a ceramic boat situated at the left side (upstream) of the tube. The substrates on the holder were located at the right side of the tube (downstream). The schematic represents the optimized location of both boats in our fabrication system.

2.2.2 ZnO NWs Deposition Conditions

The interdependence relations between the variables in the deposition are shown schematically in **Figure 2.3**. From the experience of catalytic Au thin film assisted ZnO NWs growth we can learn that catalyst thickness, substrate and Zn powder temperature, gas carrier flow rate and O₂ partial pressure are the key variables.

The catalyst (Au) thickness can affect the diameter of the ZnO NWs. The trend is the thinner Au film is, the smaller the ZnO NW diameter will be. The programmed growth temperature also changes the ZnO NWs' diameter. When the growth temperature is increased to melt the Au thin film layer, the Au liquid drops form due to the surface energy between Au melt and the substrate. If the Au layer is thin enough, the drops may separate from each other with some distance and not coalesce again. Theoretically, smaller drops can produce smaller ZnO NW diameter. The gas carrier is the media to transport the Zn vapor from upstream to the downstream of the tube. The flow rate will determine how long the Zn vapor will be heated and Zn vapor density in the tube and also the reaction time with the oxygen in the fabrication system (depending on O₂ partial pressure). The variables are closely related to each other and can make huge difference in results such as the length, density, diameter and the alignment of the ZnO NWs.

In our deposition system, the optimized variables and steps that produced vertical, dense, uniform and with selective-area growth of ZnO nanowires are: 0.2 ~ 0.5g zinc powder as source material and placed at 1/4 of the distance from the left edge of the tube, the Si substrate with pre-deposited Au or DLC film was located on the other side of the furnace in the lower temperature zone where the temperature ranges from 700 to 750 °C when the programmed temperature is set to 850 °C to 900 °C. The distance between the boat containing the Zn metal powder and the one with the substrate is another crucial variable. The furnace temperature is ramped up at a rate of 30 °C/min and held at the target deposition temperature for 30 mins, then the

temperature is ramped down at the same rate. During nanowire growth, the ambient carrier gas in the tube is controlled to have 20 sccm of Ar flow and 2 sccm of O₂ flow.

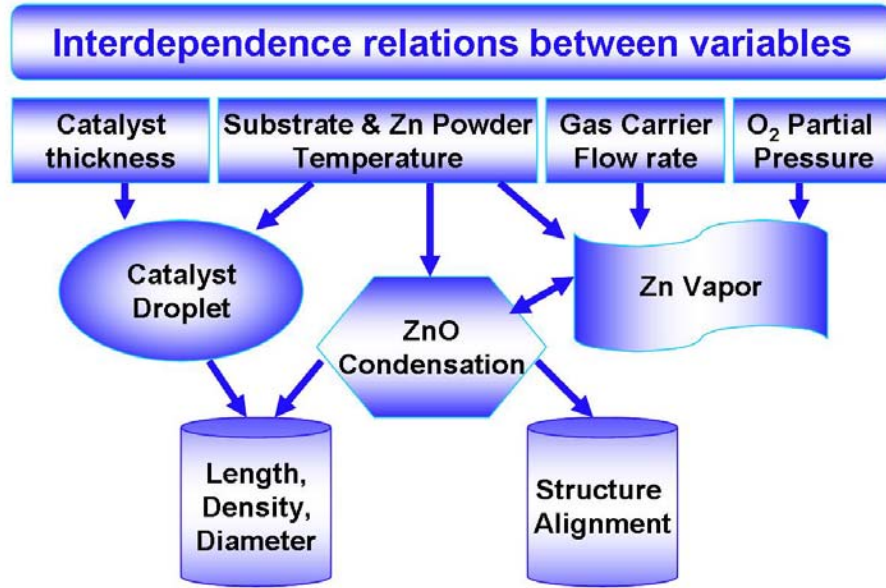


Figure 2.3 The interdependence relations between variables. The main variables are catalyst thickness, substrate, Zn powder heating temperature, gas carrier flow rate, and oxygen partial pressure. All the variables are closely related to each other and can make huge difference in results such as the length, density, diameter and the alignment of the ZnO NWs.

2.3 Characterization of ZnO NWs

2.3.1 Scanning Electron Microscopy (SEM)

The morphology of the ZnO NWs was examined by scanning electronic microscopy (SEM) that scans the sample surface with a focused electron beam interacting with the atoms in the sample. Both a Philips Electroscan E-3 Environmental SEM (ESEM), which can avoid the accumulation of electric charge on

the surfaces of non-metallic specimens, and a Hitachi SU-70 Field Emission SEM (FESEM) for higher resolution morphology examination were used in this research. In a typical SEM, electrons are emitted from a tungsten filament cathode and are accelerated towards an anode. Tungsten is normally used as a filament of the emitting gun because it has the highest melting point and lowest vapor pressure of all metals. Lanthanum hexaboride (LaB_6) is also a very common filament material used as the electron gun if the vacuum system is upgraded. Electrons can also be emitted using a field emission gun (FEG) and can provide a more coherent beam of electrons with very stable energy. This gives rise to a higher resolution image. The filament may be a cold-cathode type or a thermally-assisted Schottky type.

The electron beam in SEM facilities has an energy ranging from a few hundred eV to 40 keV, is focused by one or two condenser lenses into a beam with a very fine focal spot sized of 0.4 nm to a few microns. When the primary electron beam interacts with the sample, the electrons lose energy by repeated scattering and absorption within a teardrop-shaped volume of the specimen known as the interaction volume, which extends from less than 100 nm to around 5 μm from the surface. The energy exchange between the electron beam and the sample results in the reflection of electrons by elastic scattering, emission of secondary electrons by inelastic scattering and the emission of electromagnetic radiation which can be detected to produce an image. The image displayed is therefore a distribution map of the intensity of the signal being emitted from the scanned area of the specimen. The image may be captured by photography from a high resolution cathode ray tube or digitally captured and displayed on a computer monitor.

2.3.2 Atomic force microscopy (AFM)

Atomic force microscopy (AFM) is also used to scan the surface morphology of a sample from a measurement of the forces between a cantilever tip and the sample surface. The AFM scans over a surface by using a fine ceramic or semiconductor tip. Typically, the tip is located at the end of a cantilever with a laser beam focused at the end of the cantilever. As the tip is either repelled by or attracted to the sample surface, the cantilever deflects which results in a change of the reflected laser beam position on a photodiode. The top half and bottom half of the photodiode detect normal and shear motions, respectively by the laser displacement along the x axis of the photodiode. A plot of the laser deflection versus tip position in the x, y, and z directions on the sample surface provides 2 or 3 dimensional surface images. A sensitive piezoelectric element controls the position and motion of the tip over the surface of the substrate.

An image of the surface topography is obtained by tracking the deflection of the cantilever as it is scanned over the surface. Hooks law and Coulomb forces are involved to maintain the same force/distance between tip and sample surface and they can be written, respectively.

$$F_H = -kx, \quad (\text{Hook's Law})$$

$$F_C = \frac{q_1 q_2}{4\pi\epsilon_0 r^2}, \quad (\text{Coulomb force})$$

where k represents the elastic (spring) constant and q_1, q_2 are the charges of the tip and sample and, x, r is the distance between the tip and the sample. However, in contact mode the tip may cause damage to the sample. In some cases, non-contact

mode is used to investigate sample with soft surfaces. In non-contact mode, the sample is either held at a constant distance from the sample surface (STM mode) or the tip oscillates at a constant frequency as it is scanned on the surface (tapping mode). In this work, a Dimensions 3000 AFM was used to characterize the surface morphology.

2.3.3 Photoluminescence (PL)

Luminescence or light emission from any process other than blackbody radiation is a non-equilibrium process for it needs an excitation source, such as a lamp or a laser. With different excitation sources, we may have different kinds of luminescence: (i) *Photoluminescence (PL)* (needs optical excitation), (ii) *Electroluminescence (EL)* (requires excitation by electrical current), (iii) *Cathodoluminescence (CL)* (results from electron bombardment).

The simplest photoluminescence process is resonant radiation, in which a photon of a particular wavelength is absorbed and an equivalent photon is immediately emitted. This process involves no significant internal energy transitions of the chemical substrate between absorption and emission and the process is in the order of 10^{-8} seconds long [39]. PL is one of the most common experimental methods for study of semiconductors, especially wide-band-gap materials and mainly it has two types: intrinsic and extrinsic luminescence. The recombination of an electron in the conduction band with a hole in the valence band generates intrinsic band-to-band transition luminescence (at low temperature, this process is often replaced by the intrinsic exciton luminescence). The light emission in light-emitting diodes and

semiconductor lasers is usually the case where band-to-band transition processes take place.

A simple set-up of photoluminescence (PL) (Laser Science, Inc, Model VSL-337 ND-S, 337 nm, 6mW and Ocean Optics SD5000 spectrometer) was used for detecting the photoluminescence or light emitting properties of ZnO NWs in our study.

2.3.3 X-ray Diffraction (XRD)

X-ray diffraction (Siemens D5000 Diffractometer) is used for the ZnO NWs' structural characterization. Powder diffraction (XRD) characterizes the crystallographic structure, gives an estimate of the crystallite size (grain size) and is useful in identifying known materials, characterizing new materials and in discerning materials that appear similar by other experiments. The theory is based on the elastic scattering of x-rays from structures that have long range order. A regular array of lattice structure produces a regular array of spherical waves. Although these waves cancel one another out in most directions (destructive interference), they add constructively in a few specific directions, determined by,

$$2d\sin\theta = n\lambda, \quad (\text{Bragg's law})$$

where n is any integer, d is an interplanar distance in the sample, θ is the angle of incidence of the x-ray beam with the surface of the sample and λ is the wavelength of the incident X-ray beam. These directions appear as spots on the diffraction pattern. Thus, X-ray diffraction results from an electromagnetic wave (the X-ray) impinging

on a regular array of the repeating arrangement of atoms within the crystal. The most comprehensive description of scattering from crystals is given by the dynamical theory of diffraction that describes the interaction of wave fields with a regular lattice. Thus, we can have some information from XRD analysis, such as phase identification, crystallinity, lattice parameters, phase transitions, and crystal structure determination.

2.3.5 Transmission electron microscopy (TEM)

Transmission electron microscopy (TEM) was performed to characterize the microstructure of the ZnO NWs. TEM can be used to demonstrate the crystallinity (single crystal ZnO NWs) and the nanostructure of the NWs and the Au or DLC thin films underneath. A JEOL 2100F field emission TEM was utilized in this study.

A TEM operates similarly to an optical microscope, except that optical microscopes use light sources and focus light beams with glass lenses, while TEMs use electron sources and focus electron beams with electromagnetic lenses. The electrons emitted from a filament are accelerated by a high voltage (100 kV – 1000 kV) and focused through a set of condenser lenses onto the specimen. The electron beam is scattered by the specimen. The diffracted beams are then brought to focus by the objective lens on its back focal plane and form a diffraction pattern. A final TEM image or diffraction pattern can be produced on a fluorescent viewing screen by a series of objective lens, intermediate lens and projector and magnifying lenses. Besides diffraction and spatial imaging, the high-energy electrons in TEM cause electronic excitations of the atoms in the specimen. Two important spectroscopic

techniques make use of these excitations, i.e. energy-dispersive x-ray spectroscopy (EDS) and electron energy-loss spectroscopy (EELS). In this study, the conventional bright-field and dark-field imaging, selected area diffraction (SAD), and high resolution TEM are used to study the microstructures and energy dispersive X-ray spectroscopy (EDS/EDX) and electron energy loss spectroscopy (EELS) are used to study the chemical compositions of the films and nanowires. EDS uses detection equipment to measure the energy values of the characteristic x-rays generated within the sample. The electron microscope should be equipped with a semiconductor material device to detect the x-rays and a multichannel analyzer, an x-ray microanalysis system to convert the x-ray energy into an electronic count (intensity). The accumulation of these energy counts creates a spectrum representing the chemical analysis of the sample. Therefore, when the electron microscope produces an image of the sample's topography, energy dispersive x-ray microanalysis can reveal what elements are presented in the sample. The electron energy loss spectroscopy (EELS) available in the FETEM was used as a complementary tool to energy-dispersive x-ray spectroscopy (EDS) to also confirm the elements within the sample.

Chapter 3

Results and Discussion

3.1 Au Thin Film Assisted ZnO NWs Growth

3.1.1 Growth Parameters

Au pre-deposited thin layer on Si (001) substrate has generally been used as a catalyst to grow ZnO NWs. The Au catalytic thin layer provides nucleation sites on the substrate to improve ZnO NWs fabrication. We started this project using Au layer to find out the best growth condition in our fabrication system and then transfer the optimized growth condition to the growth of the ZnO NWs on DLC thin films.

In addition to the catalytic layer, the experiment parameters also include: carrier gas flow rate (sccm), oxygen partial pressure (P_{O_2}), crystal tube diameter (cm), Au film thickness (nm), source material (Zn powder, g) heating temperature ($^{\circ}\text{C}$), substrate temperature ($^{\circ}\text{C}$), distance between source material and substrate (cm), deposition duration (mins), temperature heating ramp speed ($^{\circ}\text{C}/\text{min}$) and cooling ramp speed ($^{\circ}\text{C}/\text{min}$). The interdependence relations between the variables in the deposition are shown in Figure 2.3.

The carrier gas flow rate was varied from 1000 sccm to 10 sccm with various oxygen partial pressure ratios ranging from 0.1% to 50% in various combinations. Au

film thickness ranged from 0 ~ 100 nm and was predeposited on the Si substrates utilizing PLD to find out the thickness dependence growth. A programmed fabrication system temperature was set from 550 ~ 1100 °C. Heating ramp and cooling ramp were fixed to 30 °C/min and 50 °C/min respectively. ZnO NW deposition duration was 30 mins. From our results, as for ZnO NWs deposition duration, the ZnO NWs reveal visible length in the SEM after 5 mins of growth.

3.1.2 Temperature Dependence

The interdependence relations among all the variables were tested in our NWs growth system. For the best result, the Zn powder source material was set at left side ~1/4 length measured from the beginning of the filament heating zone (see Figure 2.2) and the temperature zone was the same as the set temperature. However, the substrates had better growth with clean, dense, vertically oriented ZnO NWs when they were located at the right end of the filament heating zone where the temperature was 100 to 150 °C lower than the programmed temperature. The temperature gradient and the best growth zone are shown in Figure 2.2. The experiments for **Figure 3.1 (a) ~ (d)** have all parameters but substrate temperature fixed. The figures show that ZnO NWs start to grow when the programmed temperature is set to 600 °C to 900 °C while the substrates actual temperature were of 500 °C (a) to 800 °C (d) respectively. There is a trend in the images in Fig. 3.1; with increasing growth temperature, the NWs have thinner diameter. The diameter can be varied from ~20 nm to ~1000 nm. However, if the temperature is too high, higher than 1100 °C, the growth condition was changed to random NWs growth or no growth at all. Over all, the best growth

furnace temperature for dense, smaller diameter, vertically oriented and uniformly distributed NWs growth is around 850 to 950 °C for our evaporation system where the substrate temperature was from ~700 to ~850 °C. The uniformity of the ZnO NWs is also getting better when we increase the NW growth temperature. The ZnO NW density is also increased when the growth temperature is increased.

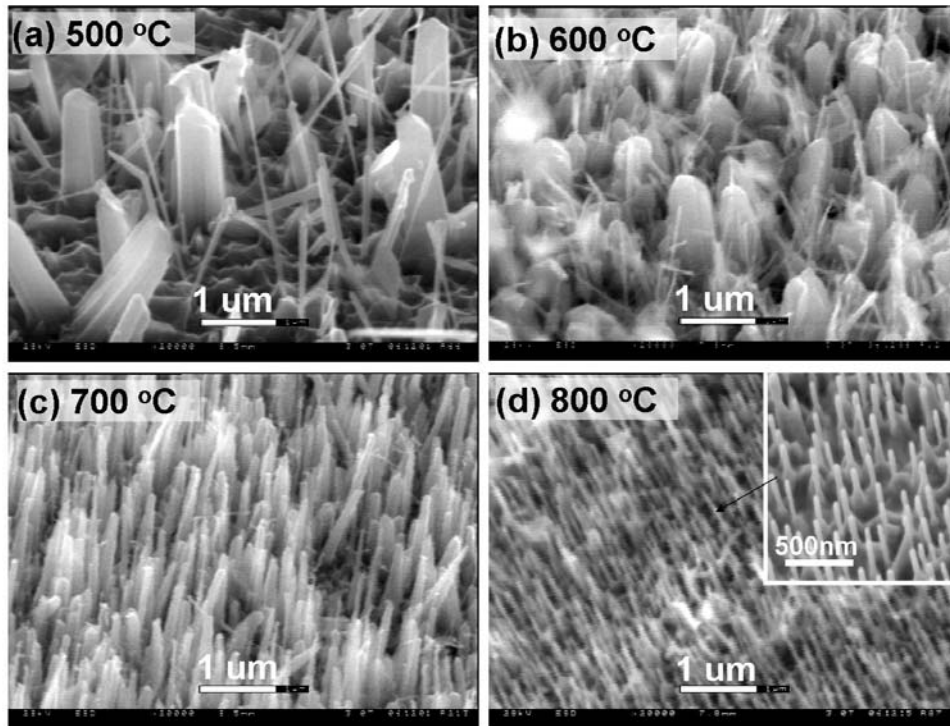


Figure 3.1 (a) ~ (d) ESEM (ESEM stage 45° tilted) sample images show the ZnO NWs growth results at various substrate temperatures (from 500 ~ 800 °C). The ZnO NW growth temperature is the only variable here. We can see the trend of the NWs' diameter is decreased when the substrates temperature was increased. The diameters decreased from μm range to tens of nm range. The inset in (d) is a magnified FESEM image of the NWs. The uniformity of the ZnO NWs is also getting better when we increase the NW growth temperature.

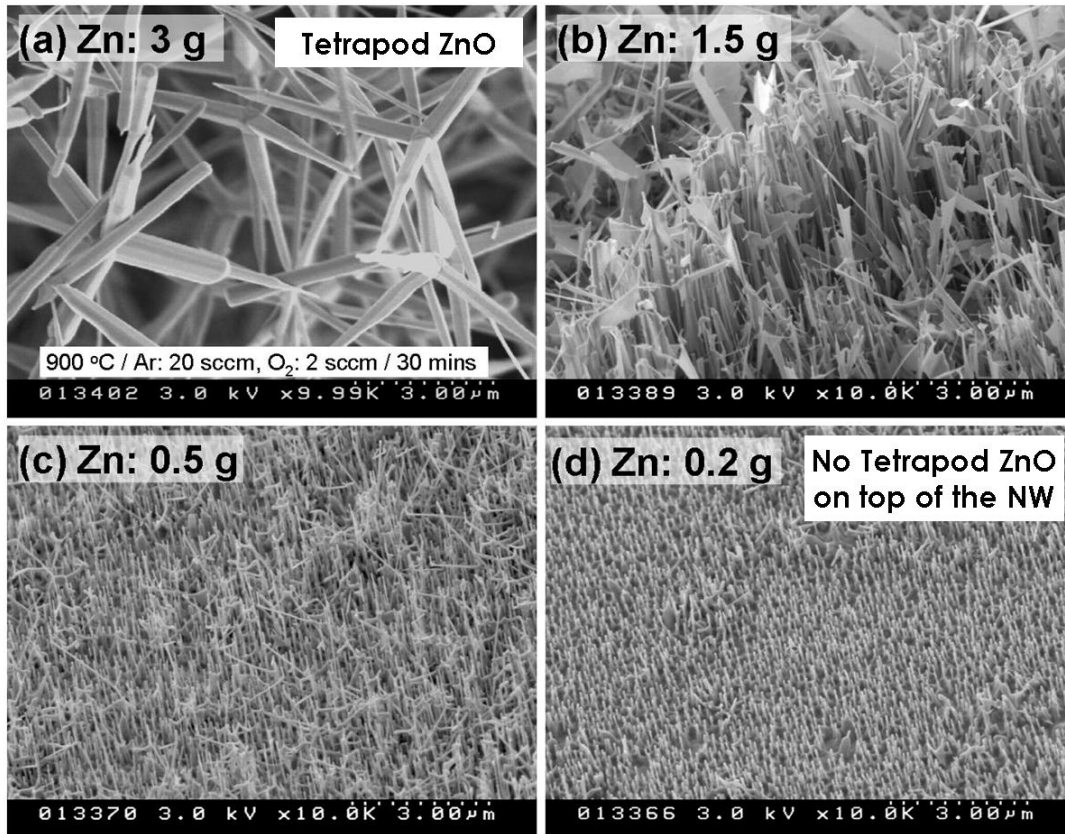


Figure 3.2 (a) ~ (d) FESEM images for varying Zn powder weight from 3g to 0.2g. Image (a) is covered by dense tetrapod shape ZnO added-on by deposition on top of the substrate surface. Images (b) and (c) have less and less unwanted deposition on top of the ZnO NWs. (d) When the Zn weight reduces to near 0.25 ~ 0.2g, nanowires with uniform diameter, and vertically oriented grow on the substrate surface.

3.1.3 Zn Weight Dependence

When Zn powder is evaporated and carried through the tube by the carrier gas to the surface of the substrate located downstream in the tube the deposition begins. The Zn vapor may have already reacted with the oxygen and form ZnO in the vapor. When Zn/ZnO vapor is transported to the lower temperature heating zone it is

deposited on the substrate surface and the ZnO NWs start to grow. The amount of Zn powder directly contributes to the Zn vapor in the tube. Excessive Zn vapor in the tube results in unwanted add-on tetrapod shape ZnO deposition over the substrate surface. **Figures 3.2 (a) ~ (d)** are FESEM images of ZnO NWs grown with various amounts of Zn powder. Figure 3.2 (a) corresponds to excessive Zn amount and consequently produces dense tetrapod shape ZnO deposition over the surface of the substrate. Images (b) and (c) show less and less unwanted deposition on top of the ZnO NWs while we tried to reduce the Zn weight. When the Zn weight decreases to 0.25 ~ 0.2 g, most of the add-on ZnO is eliminated (image (d)) and it reveals nanowires with preferred orientation, high density, small diameter, vertically oriented and uniformly distributed on the substrate.

3.1.4 Gas flow Dependence

Gas flow (sccm) and oxygen partial pressure (P_{O_2}) are other important parameters in the growth of the nanowires. In our experiments, the best ZnO NWs were obtained for total gas flow between 18~ 28 sccm. In our ZnO NWs growth (Figure 3.2 (d)), we set the gas pressure at 20 sccm of Ar and 2 sccm of O₂ which gives a total gas pressure of 22 sccm and the oxygen partial pressure to be 9.09% .

3.1.5 Au Thin Film Thickness Dependence

Another important parameter that determines the diameter of the nanowires is the thickness of the catalyst Au layer. Many researchers have demonstrated that the Au thickness is the key parameter for the NWs growth. At the furnace heating temperature, Au catalyst thin layer may melt and become a Au drop. The size of the drop determines the ZnO NWs' diameter. Theoretically, the thinner the Au layer is, the smaller the NWs diameter is. It is suggested that when the substrate was heated in the fabrication system, the nanometer thick Au film will be melted and turn into nanosized Au nanoparticles that provide the nucleation sites (**Figure 3.3**). From our result, there exists a critical thickness of Au layer of about 10 nm. A Au layer thinner than 10 nm produces more uniform ZnO NWs. The thinner (down to 1 nm in thickness) the Au layer is; the better growth of the nanowires will be. On the other hand, a thicker Au predeposited layer may result in growth of random size and shapes of nanowires with wider range of diameters. A schematic showing the Au layer and the ZnO growth conditions is presented in **Figure 3.4**. In the case of using Au layer as the catalyst layer for ZnO NW growth, only the very thin Au layer area can produce uniform, dense, and vertically aligned ZnO NWs.

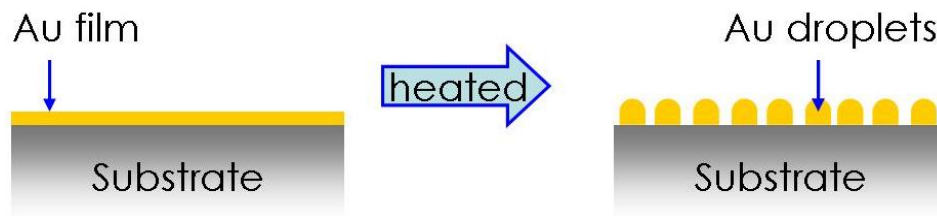


Figure 3.3 When the substrate is heated in the fabrication system, the nanometer thick Au film melts and turns into nanosized Au particles that act as nucleation sites for the growth of the nanowires.

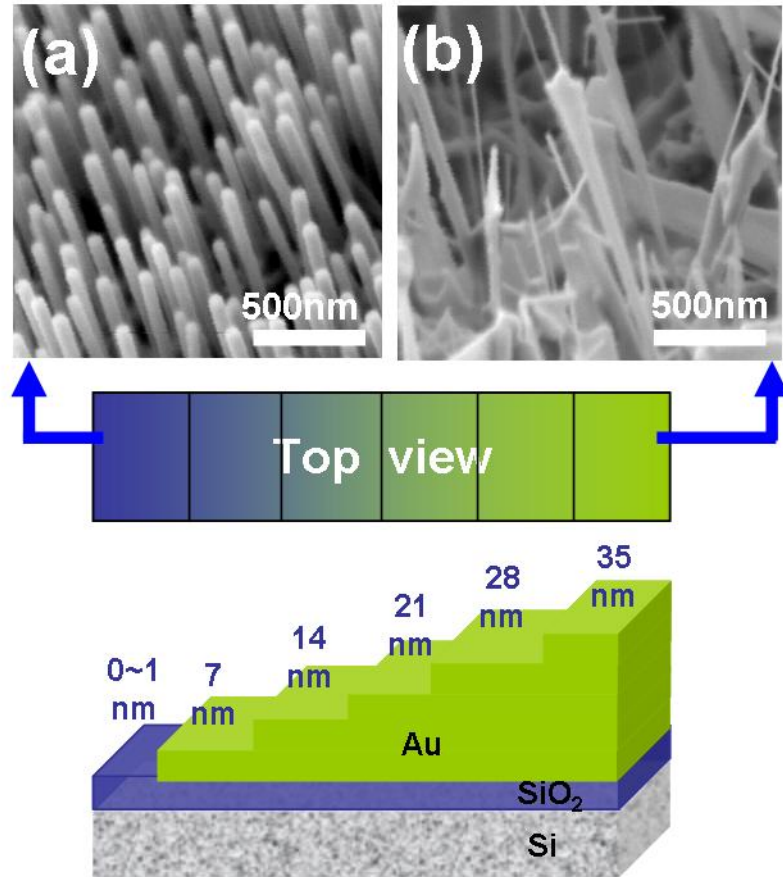


Figure 3.4 Schematic (bottom) of Au catalyst layer with gradient thickness and its dependence on the ZnO NWs growth. SEM image (a) is the NWs growth on thinner (0~10 nm) Au layer where the ZnO NWs grow vertically and uniformly. Image (b) represents the morphology of the growth at the thicker (> 15 nm) area where the ZnO has various shapes and diameters.

3.1.6 Optimized Growth Condition

Based on the variation of density, diameter and uniformity of the NWs presented in the previous section, we selected the optimum growth parameters and steps as follows: Preparing Si (001) substrate and depositing 1~ 5 nm Au thin layer utilizing PLD. Weighing Zn powder – 0.20 ~ 0.25g and put it in a ceramic boat

situated at the left 1/4 of the crystal tube, the substrates were placed on another boat at the right end (downstream) of the tube. The two boats were separated from each other by about 20 cm. A mixture of Ar + O₂ is used as carrier gas in the fabrication system with flux of 20 sccm and 2 sccm, respectively.

Figure 3.5 shows the SEM images taken from nanowires grown near the optimized conditions. By changing the growth parameters, we can have different ZnO NWs morphologies. Images (a) and (b) in Figure 3.5 are ZnO nanowires grown on 5 nm thick Au layer on Si substrate. Images (c) and (d) are the growth on 1 nm thick Au layer Si substrate. The Au layer thickness results in different ZnO nanowire length and density. We get longer (~200nm NW on 5 nm thick Au layer, and >1000 nm long on 1 nm thick Au layer) nanowires in thinner Au layer predeposited on the Si substrate. It's widely suggested that when the Au layer is thicker, it takes more Zn to saturate the Au layer/drop. After Au layer/drop is oversaturated, the ZnO nanowire growth begins.

Optimized ZnO NW Growth Condition on Au Layer

- ◆ Au thickness : 1 nm
- ◆ Zn source material heating temperature: 900 °C (Zn Weight: 0.25 g)
- ◆ Ar/O₂: 20/2 sccm (P_{O₂}: 9.09%)
- ◆ Temperature Ramping (heating/cooling): 30/50 °C/min
- ◆ Growth time: 30 mins (shows visible NWs >50nm long after 5 mins growth)

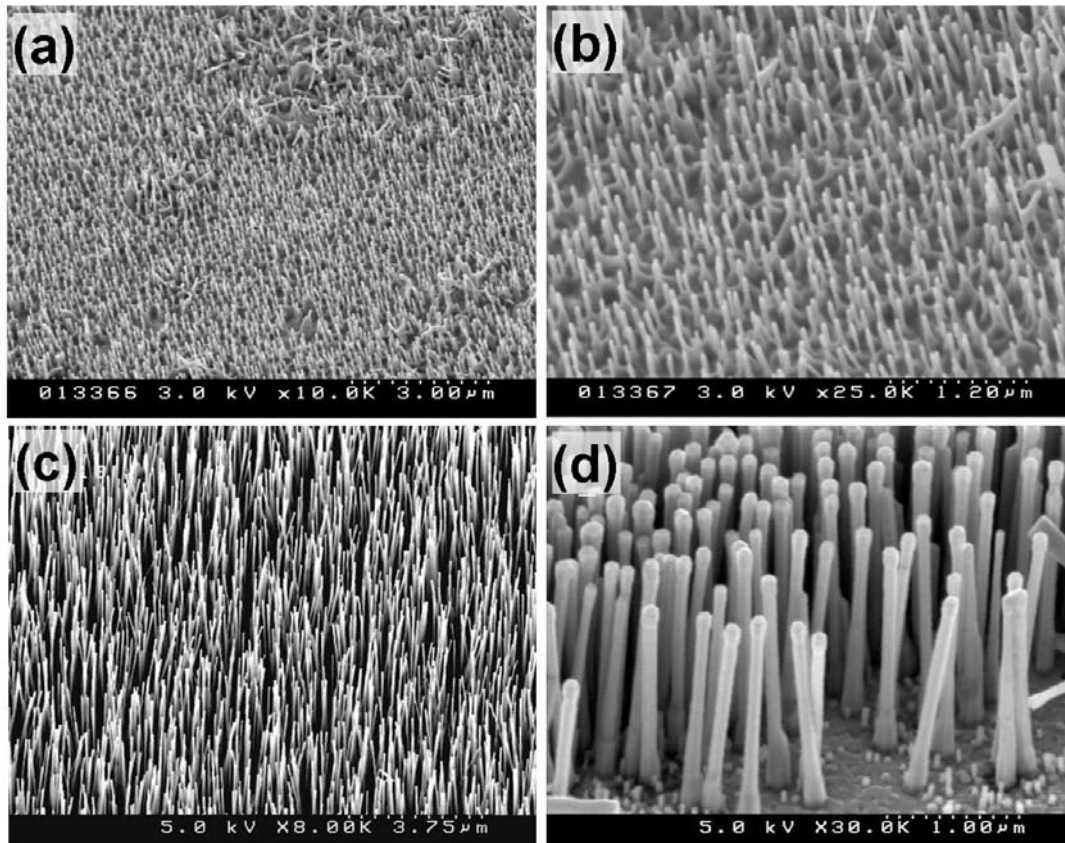


Figure 3.5 SEM images taken from nanowires grown with optimized parameters but different predeposited Au layer thickness on Si (001) substrate. Images (a), (b) are for 5 nm thick Au layer and images (c), (d) are for 1 nm thick Au film. The nanowires' length increases from ~200 nm in (a), (b) to > 1000 nm in (c), (d).

Figure 3.6 shows a schematic of the predeposited and patterned Au layer on the Si substrate (top view) and the SEM image of the ZnO NWs selectively grown on 1nm and 10nm thick Au pre-deposited layer. The two regions are separated by a region of bare SiO₂ on Si substrate. After 30 mins of growth at 900 °C, the area with 1 nm Au catalytic thin film has denser, more uniform and vertically oriented growth compared to the region with 10 nm Au layer. This result shows the thickness dependence and also the selectivity (Au layer region) of the growth where the bare SiO₂ region has very clean surface without nanowire growth.

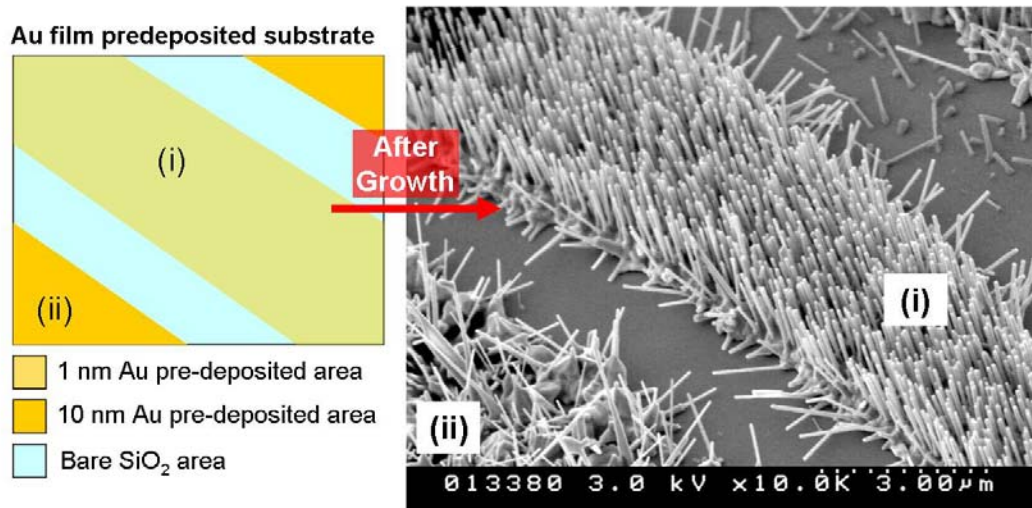


Figure 3.6 Schematic and SEM image of the ZnO NWs selective growth with 1nm and 10nm Au thin film. The ZnO NWs grown on 1nm thick Au layer shown in area (i) in the SEM image. The NWs in this area are well-aligned and uniform. The growth in area (ii) is much more random and there is no preferred orientation. The bare SiO₂ area is very clean with almost no nanowire growth.

3.2 DLC Thin Film Assisted ZnO NWs Growth

ZnO is an n-type, direct wide bandgap (~ 3.37 eV) semiconductor and has potential for the fabrication of light emitting diodes, sensors and UV laser diodes due to its large exciton binding energy (~ 60 meV) which is more than twice the thermal energy at room temperature. There is also a great interest in nano-structured carbon films for their potential use as cathodes in field emission displays (FEDs); note that DLC can be fabricated at room temperature by plasma deposition technique at low cost. A remarkable enhancement of the field emission of nanocomposites of ZnO NWs on amorphous diamond film was found compared to that of the intrinsic amorphous diamond [40]. However, there is no report so far of successful growth of

uniform, vertical, and well aligned ZnO NWs fabricated on top of diamond-like carbon thin films. In this study, we applied our deposition experience from Au catalyst layer growth to fabricate ZnO NWs on top of DLC films. In this section, we demonstrate that ZnO NWs can be fabricated on DLC films under certain growth parameters with uniform, well aligned and controllable density. The results open up the potential applications of ZnO NWs as cold cathodes in field emission displays using this ZnO NWs / DLC film growth geometry.

3.2.1 DLC Film Deposition Temperature Dependence

For DLC film assisted growth, we used pulsed laser deposition (PLD) to pre-deposit ~25 nm DLC film at various substrate temperatures. Over the DLC film ZnO NWs were grown using the same parameters used for Au assisted NW growth. The common fabrication of ZnO NWs in the chemical vapor transport and condensation (CVTC) growth system usually has ZnO powder and graphite as a mixture as the source material [3-20]. The carbon content was proposed to play an important role in the redox process during the growth of the NWs. The DLC films were usually composed of crystalline graphite with sp^2 bonding and amorphous carbon with sp^2 and sp^3 bonding. Note that graphite is 100% sp^2 bonding, diamond is 100% sp^3 bonding and that of DLC is in between. It's known that there exists a trend for DLC film deposition that the lower the deposition temperature, the higher the sp^2/sp^3 bonding ratio [36, 38].

Different ZnO nanostructures with different morphologies were obtained in this case as shown in **Figures 3.7 (a) ~ (d)**. The ZnO NWs growth parameters are: 0.25 g

of Zn weight and 900 °C Zn source temperature and total carrier gas Ar/O₂ flow of 22sccm (20/2 sccm of Ar/O₂). Figure 3.7 (a) is a schematic of the deposited DLC pattern; each pad is about 100 μ m \times 100 μ m in width and length and 25 nm in thickness. Figures 3.7 (b) ~ (d) are SEM images (SEM stage has a tilted angle of 45°) of the ZnO NWs growth morphologies on top of the DLC films which were deposited utilizing PLD at room temperature, 400 °C and 600 °C, respectively.

SEM images (b) ~ (d) show the influences of DLC film deposition temperatures to the ZnO nanowires growth and reveal that the nanowires' length has the trend of (b) > (c) > (d). This result may be due to the DLC film deposited at 600 °C has less graphite sp² portion and result in shorter NWs length; probably because of insufficient carbon to participate in the redox process after a period of time during growth. We should also note that the density of the NWs is also affected by the quality of DLC film which may open up the opportunity of controllable density by changing the pre-deposited DLC film. A growth mechanism in the current work will be discussed later in chapter 4.

Figure 3.8 top view SEM images (a) ~ (f) are a comparison of ZnO NWs' density grown on DLC films deposited at various-temperatures (R.T., 200 °C and 400 °C). The ZnO NWs growth condition shown in images (a) ~ (f) were fabricated under the same growth parameters (0.25 g of Zn weight and 900 °C Zn source temperature and total carrier gas Ar/O₂ flow of 22sccm) but the DLC film deposition temperature. The ZnO NWs density is calculated from the SEM images to be 4, 9, 12 NW/ μ m² for the growth on R.T., 200 °C and 400 °C deposited DLC film, respectively. From

these SEM images, the NWs density also increases with DLC film deposition temperature.

We should notice that from images in Figure 3.8 (b), (d) and (f), the magnified images from (a), (c) and (e), the grain size underneath the NWs also has a trend to decrease when the DLC growth temperature increase and each grain produces a nanowire on top of it. Consequently, when ZnO NWs grow on DLC deposited at higher temperature (within the range of R.T. to 400 °C), the grain size underneath the NWs will decrease, and the NWs density on top of the grain increases.

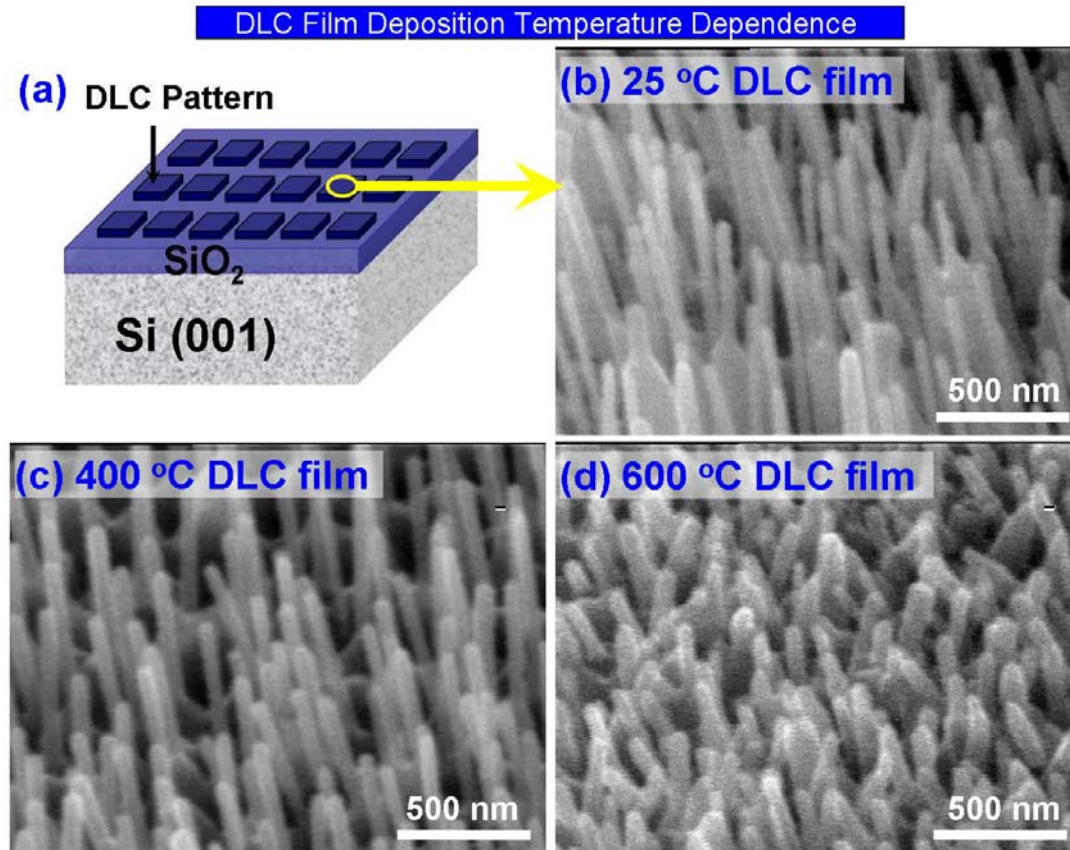


Figure 3.7 (a) Schematic of the DLC thin film pattern predeposited on SiO₂/Si (001) substrate before nanowire growth. Images (b) to (d) are the ZnO NWs growth morphology on DLC films that were deposited at room temperature (b), 400 °C (c) and 600 °C (d). The NWs length decreases when the DLC deposition temperature increases.

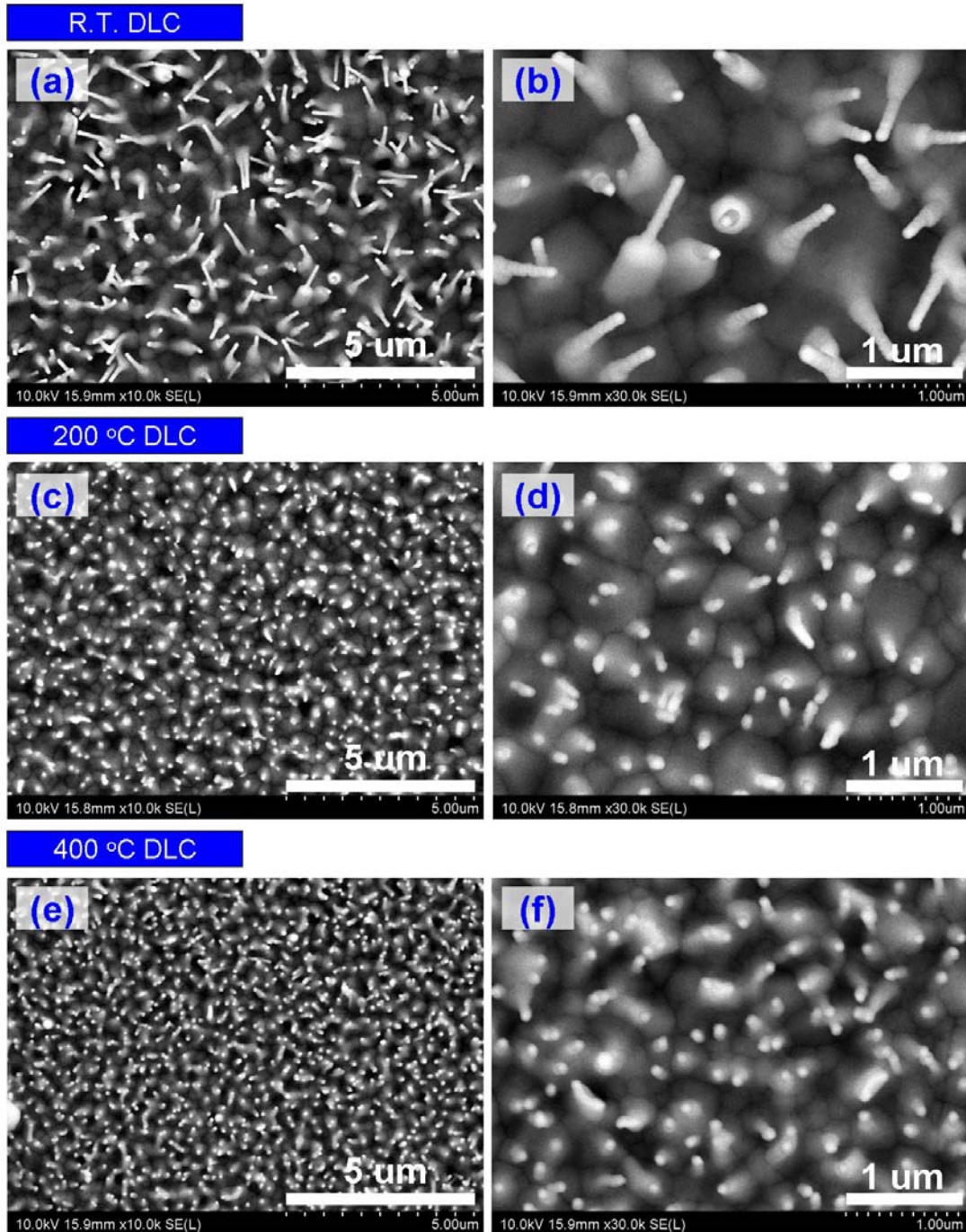


Figure 3.8 SEM images of NWs grown on DLC film deposited at R.T. (a, b), 200 °C (c, d) and 400 °C (e, f). Other ZnO NWs growth parameters were the same for all three samples. From the magnified SEM images (b), (d) and (f), we can see the ZnO grain underneath the nanowires. The grain size decreases when the deposition temperature (in the range of R.T to 400 °C) of the DLC film increases. The smaller grain size results in higher nanowire density.

3.2.2 DLC Film Thickness Dependence

To investigate the dependence of the DLC film thickness on the growth of the nanowires, we deposited the DLC film with a thickness gradient in the range of 1 ~ 100 nm along a 10 mm long Si substrate. The DLC thickness gradient was controlled by a moving shadow mask in the PLD chamber. A $100\mu\text{m} \times 100\mu\text{m}$ DLC pad pattern was also transferred to the substrate for selective area growth (**Figure 3.9**).

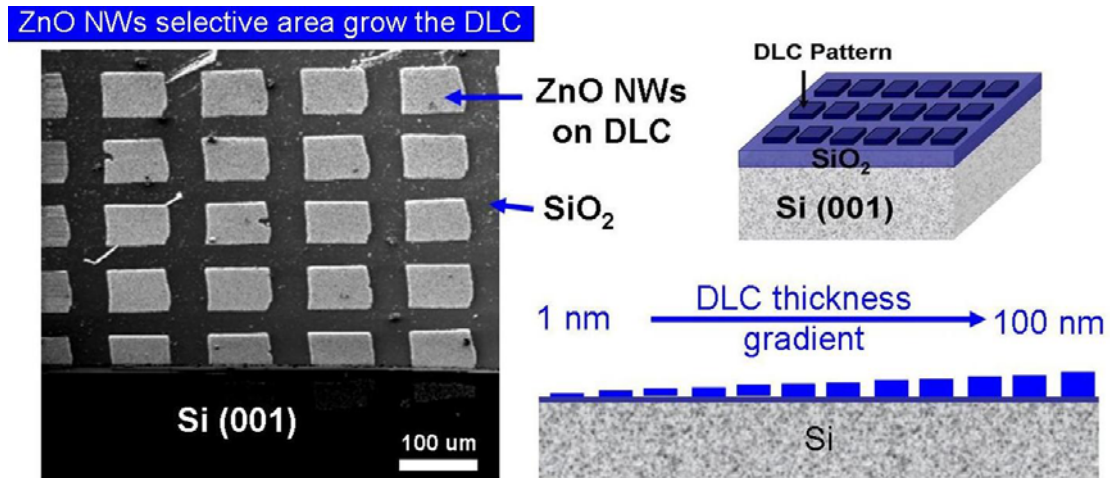


Figure 3.9 SEM image of ZnO NWs selective growth on DLC film pattern and schematics of $100\mu\text{m} \times 100\mu\text{m}$ size DLC pad pattern and a thickness gradient in the range of 1 ~ 100 nm along a 10 mm long Si substrate. The selective area growth shows the NWs preferred to grow on DLC film but not on SiO₂ surface.

Figure 3.10 presents SEM images (a) ~ (d) from the ZnO NWs with morphologies produced on DLC film with different thickness ($t_{\text{DLC}} = 1 \sim 100\text{nm}$). (The DLC film for this experiment was deposited using PLD at room temperature.) All of the images exhibit similar shape of NWs which has a thicker diameter (ϕ) at the bottom part (nanorods (NRs), $\phi_{\text{NR}} = 150 \text{ nm} \sim 500 \text{ nm}$) and then a thinner

diameter (nanowires (NWs), $\phi_{NW} = 20 \sim 100$ nm) on the upper part of the nanorods. However, the shape of the ZnO NWs and their morphologies changes when the t_{DLC} changes. Image (a) in Figure 3.10 shows the NWs deposited on thinner DLC layer ($t_{DLC} = 1 \sim 15$ nm). In this area the ZnO NWs have the NW/NR shape, from the top to the bottom, with diameter of 50 ~ 100 nm for the nanowires and 200 ~ 500 nm for the nanorods. The NWs on top of the NRs get longer with thicker DLC film ($t_{DLC} = 15 \sim 30$ nm) underneath (see Figures 3.10 (b) and (c)). However, when the ZnO NWs grow on top of the DLC film with $t_{DLC} = 30 \sim 70$ nm, the growth uniformity decreases and the nanowire portion gets shorter compared to the growth on the thinner DLC film ($t_{DLC} = 15 \sim 30$ nm) region. Interestingly, when the growth goes to the thicker, $t_{DLC} = 70 \sim 100$ nm area (see Figure 3.10 (d)), the NWs uniformity comes back and the NW become longer ($3 \sim 4 \mu m$).

Figure 3.11 shows SEM images with more detail morphology of the NW/NRs grown on the DLC region with $t_{DLC} = 1 \sim 15$ nm. Figure 3.11 (a) shows top view, low magnification of the NWs grown on $t_{DLC} = 1 \sim 15$ nm area. Images (a), (b), and (c) are normal view of the ZnO NWs at different magnifications while image (d) is the image with 50 degree sample tilt. From image (c), we can see that the NWs are faceted indicating high degree of crystallinity. From Figure 3.10 we can see that this specific growth condition produces large diameter NR and a short NW with small diameter on the upper part. The film underneath of the NRs had porous morphology which we can see in more detail in TEM cross-section examination in section 3.3.5.

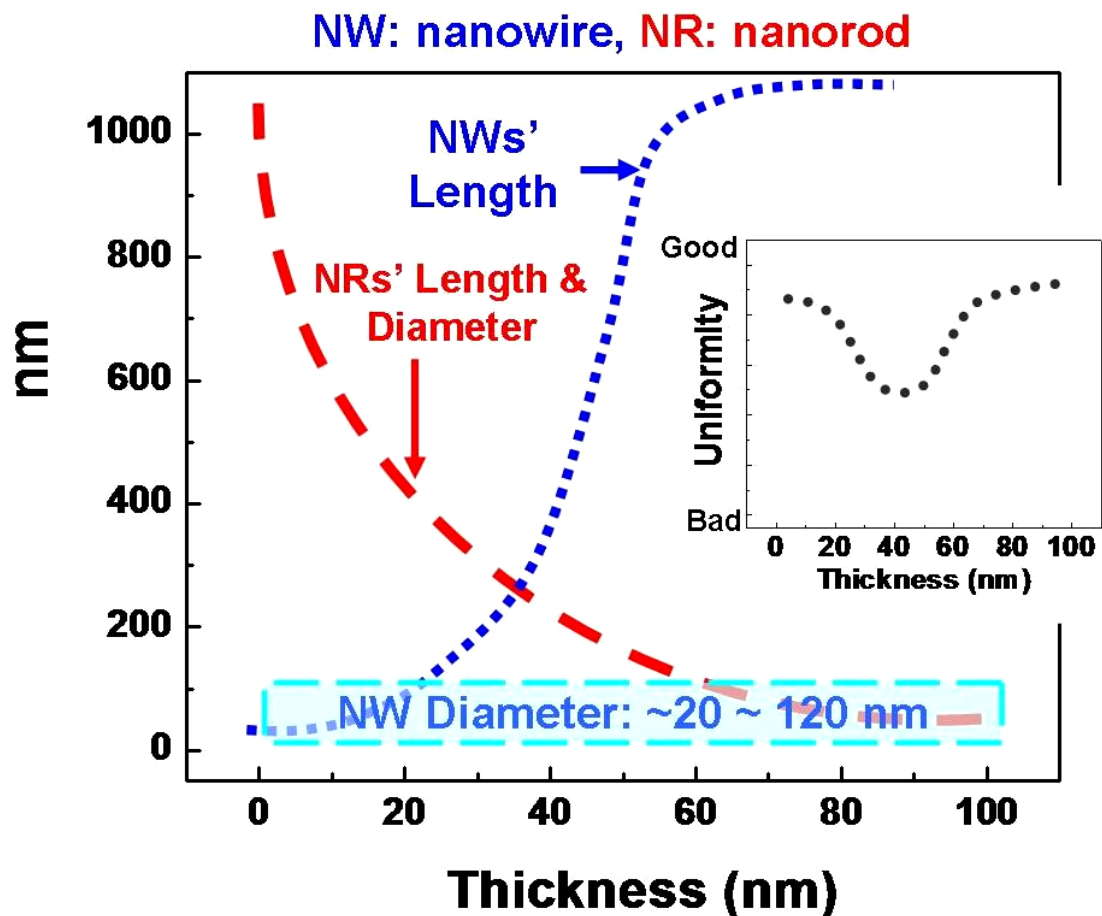
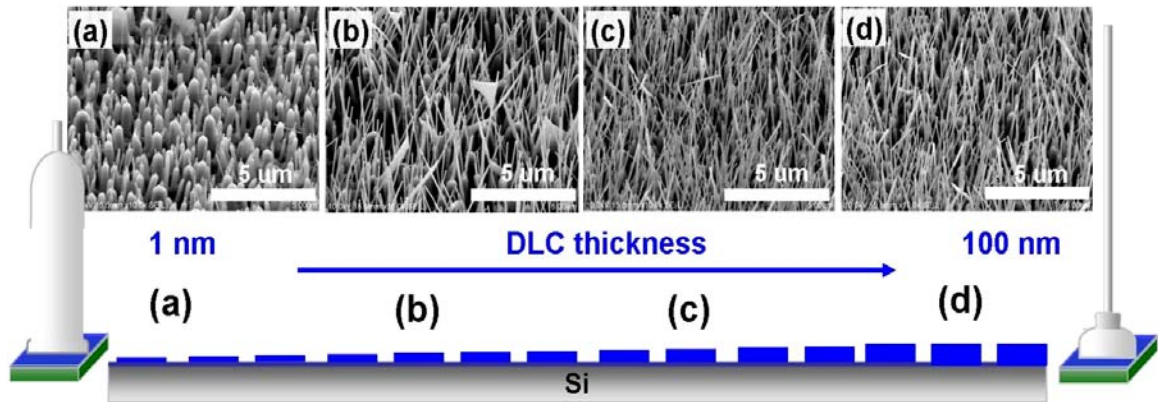


Figure 3.10 (a) ~ (d) are the SEM images of the ZnO NWs morphologies grown on different thickness (1~100nm) of DLC film of the substrate. The schematics show the changes of NW/NR length and diameters grown on different DLC thickness. The plot shows the trend of the diameter and the length of ZnO NW/NR with the DLC film thickness and the inset is the ZnO NW/NR uniformity trend. The uniformity is better when the NWs grow on the thinner (< 20nm) and thicker (> 75nm) DLC film. Note that, for this set of samples the only variable is the DLC film thickness. A change of any of the other growth parameters will have different result.

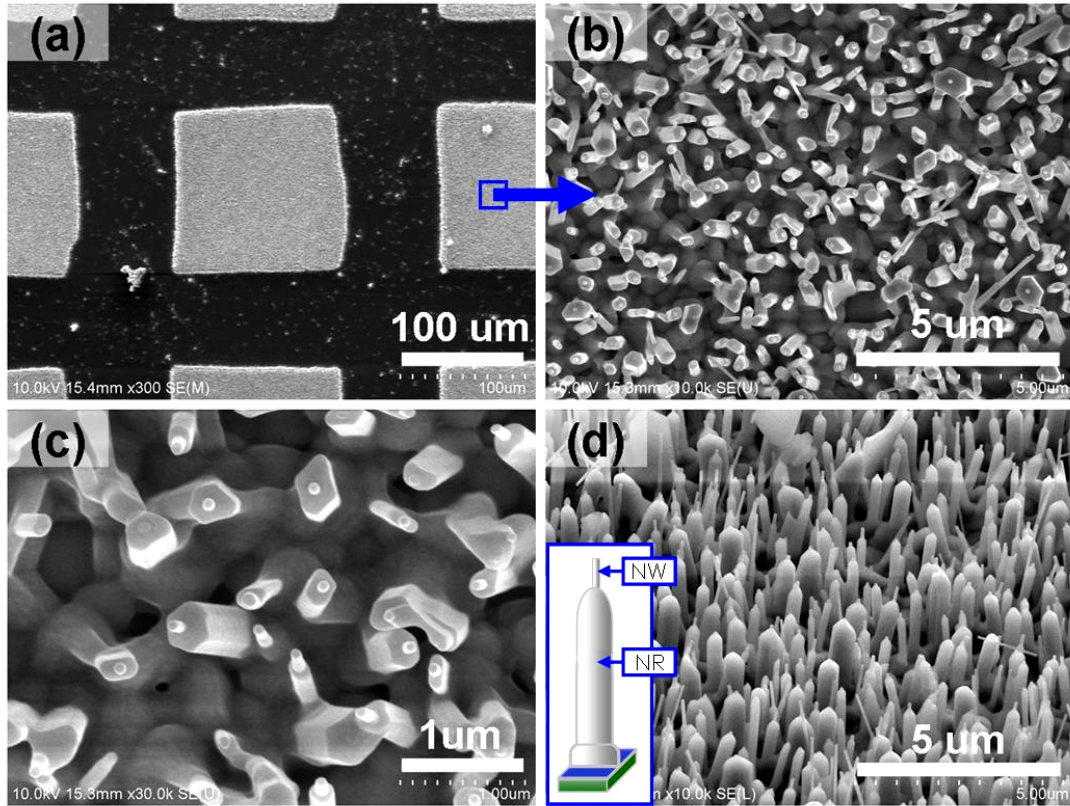


Figure 3.11 SEM images of the nanowire/nanorods morphology on the region of DLC thickness $t_{\text{DLC}} = 1 \sim 15$ nm. (a ~ c) are normal view images and (d) has a 50° sample tilt. Image (c) shows the porous morphology underneath the NRs and the NWs/NRs are faceted indicating high degree of crystallinity.

3.2.3 ZnO NWs Growth Dependence on Temperature

We investigated the effect of temperature during the fabrication system for growth of NWs from 500°C to 1150°C . The growth temperature is also a crucial parameter in growth control. From our experimental results for Au film catalyst, the Zn source (the boat that carries Zn powder) has to be placed at $1/4$ of the distance of the quartz tube in the furnace from the left edge where it will be heated at the temperature we set in the furnace. A second boat holding the substrate needed to be

located toward the end part of the right side of the quartz tube where the temperature gradient is high. The best separation between the two boats was about 10 cm and the temperature difference between the two boats is about 150 °C. In other words, when the temperature is programmed to 900 °C, the substrate has to be separated from the Zn source boat by 10 cm and located in the region where the temperature is ~750 °C (growth temperature).

The ZnO NWs started to have high degree of orientation when the fabrication system temperature was programmed to higher than ~850 °C. The comparison of the NWs grown at different temperatures is shown in **Figure 3.12**. Images 3.12 (a) to (c) are from NWs grown when the furnace heating temperature was set at 850, 900, and 1000°C, respectively. The images show the same trend as in the case of Au film assisted growth for which the diameter decreases when the growth temperature increases.

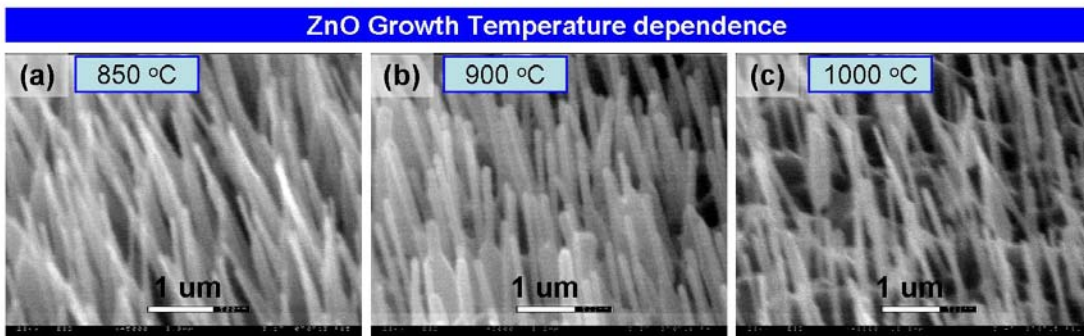


Figure 3.12 (a) – (c) shows the growth temperature dependence on the NW morphology. The growth temperature was set to 850, 900, and 1000 °C, respectively. It reveals the same trend as for Au film assisted growth for which the NWs density increases and diameter decreases when the growth temperature increases.

3.2.4 Oxygen partial pressure dependence

Oxygen partial pressure (P_{O_2}) plays a very important role in the ZnO NW growth to ensure the right stoichiometry of the NWs and the correct crystal structure. In our fabrication system, the oxygen partial pressure plus the total gas flow change the growth condition significantly. **Table 3.1** shows the growth dependence on the oxygen partial pressure (P_{O_2}). We set our carrier gas parameters for Ar/O₂ to be 20/1 ($P_{O_2} = 4.76\%$) and 20/2 ($P_{O_2} = 9.06\%$) to find out the best growth condition for our system.

Ar (sccm)	O ₂ (sccm)	P _{O₂} (%)	Total Flow (sccm)	NWs Growth [X: NO, O: YES]
15	1	3.85	16	X
15	2	11.67	17	O
15	3	16.67	18	X
20	1	4.76	21	O
20	2	9.06	22	O
20	4	16.67	24	X
25	1	3.85	26	X
25	2	7.41	27	O
25	3	10.71	28	O

Total flow from 17 ~ 28 sccm and P_{O₂} (%) from 4~11% can give vertically aligned ZnO NWs on DLC film

Optimum P_{O₂} for growth on DLC film

Optimum P_{O₂} for growth on Au film

Table 3.1 Growth dependence on the Ar/O₂ flow (sccm) and oxygen partial pressure (P_{O_2} %). In our growth system, Ar/O₂ of 20/1 ($P_{O_2} = 4.76\%$) and 20/2 ($P_{O_2} = 9.06\%$) show the most uniform and well-aligned ZnO NWs.

Taking into account the effect of all the growth parameters, we can adjust the NWs morphology, density, uniformity, length and diameter in a controlled manner. We have also determined the best conditions to obtain high density, thin and long NWs with uniform distribution. **Figure 3.13** shows SEM images of NWs grown with optimum parameters: Zn powder (0.25 g), Ar/O₂ (20/1 sccm), separation distance of Zn powder boat and substrate holding boat (10cm), Zn source heating temperature (900 °C), substrate temperature (750 °C), DLC (t_{DLC}= 25nm)/Si (001) substrate. Note that P_{O₂}, Ar/O₂ of 20/1 (P_{O₂} = 4.76%) is optimum for the NWs growth on DLC film and 20/2 (P_{O₂} =9.06%) is optimum for the NWs growth on Au film for uniform and vertically aligned ZnO NWs.

Optimized ZnO NW Growth Condition on DLC film

- ◆ DLC thickness : 25 nm
- ◆ Zn source material heating temperature: 900 °C (Zn Weight: 0.25 g)
- ◆ Ar/O₂: 20/1 sccm (P_{O₂}: 4.76%)
- ◆ Temperature Ramping (heating/cooling): 30/50 °C/min
- ◆ Growth time: 30 mins

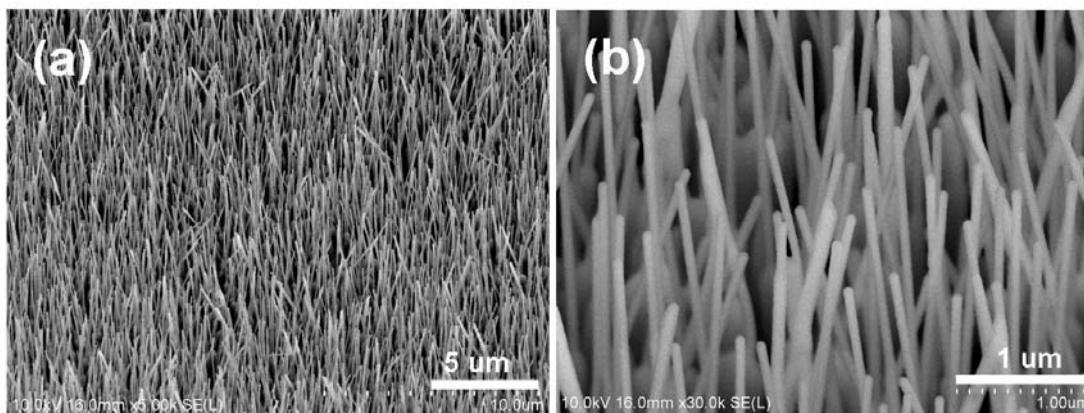


Figure 3.13 SEM images showing NWs grown on DLC film with the optimum parameters to obtain high density ($17 \text{ NM} / \mu\text{m}^2$), thin (20 nm ~ 80 nm) and long ($4 \mu\text{m}$ for 30 mins growth) NWs with uniform distribution.

3.3 Chemical, Structural and Optical characterization of ZnO NWs

Grown on DLC film

3.3.1 Energy-Dispersive X-ray Spectroscopy (EDS) Analysis

We performed extensive SEM characterization to investigate the morphology of the NWs grown on DLC film as shown in section 3.2. Schematics in **Figures 3.14 (a) ~ (d)** show the different morphologies observed in this study for different growth conditions.

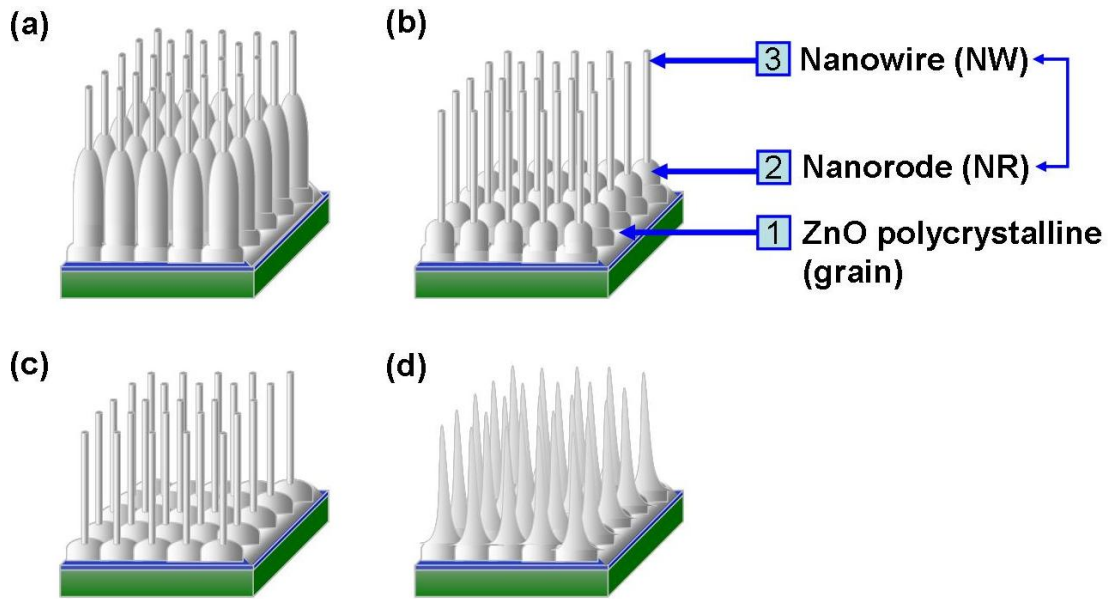


Figure 3.14 Different ZnO NWs morphologies observed in this study. There is a ZnO polycrystalline film that forms at the first stage of the growth and the NWs grow on top of it. ZnO NWs have two sections. The bottom section (nanorod) has wider diameter varying from 100 nm up to $1\ \mu\text{m}$, depending on the growth conditions. The thinner section on top uniformly grows down to $\sim 20\ \text{nm}$ in diameter and has a c -axis orientation along the growth direction. The NWs extend for $3 \sim 5\ \mu\text{m}$ in length.

These are the most common shapes of ZnO NWs observed in this study. Images (a) to (c) are the NWs with larger diameter base (nanorods, NRs) with thinner NWs on top. NWs with sharp tips shown in image 3.14 (d) are usually fabricated when the oxygen partial pressure is higher than our optimum parameter. Straight NWs with uniform diameter shape, vertically oriented growth are very common for a fairly wide range of parameters.

Figure 3.15 presents an SEM-EDS line scan from a NW. (a) is the SEM image of the scanned area with ZnO NWs on top of ZnO film/grain and DLC film underneath. The spectrum in Figure 3.15 (b) shows strong peaks of Zn, O and C. The carbon detected here more likely came from the DLC film underneath the examined ZnO NW. The line scan in Figure 3.15 (c) reveals that the ZnO NW is uniform with

Zn and O exhibiting the same signal trend while C remains fairly constant. Image in Figure 3.15 (d) is the 3 μm long single NW chosen to be examined for EDS line scan for 3 mins from bottom to top.

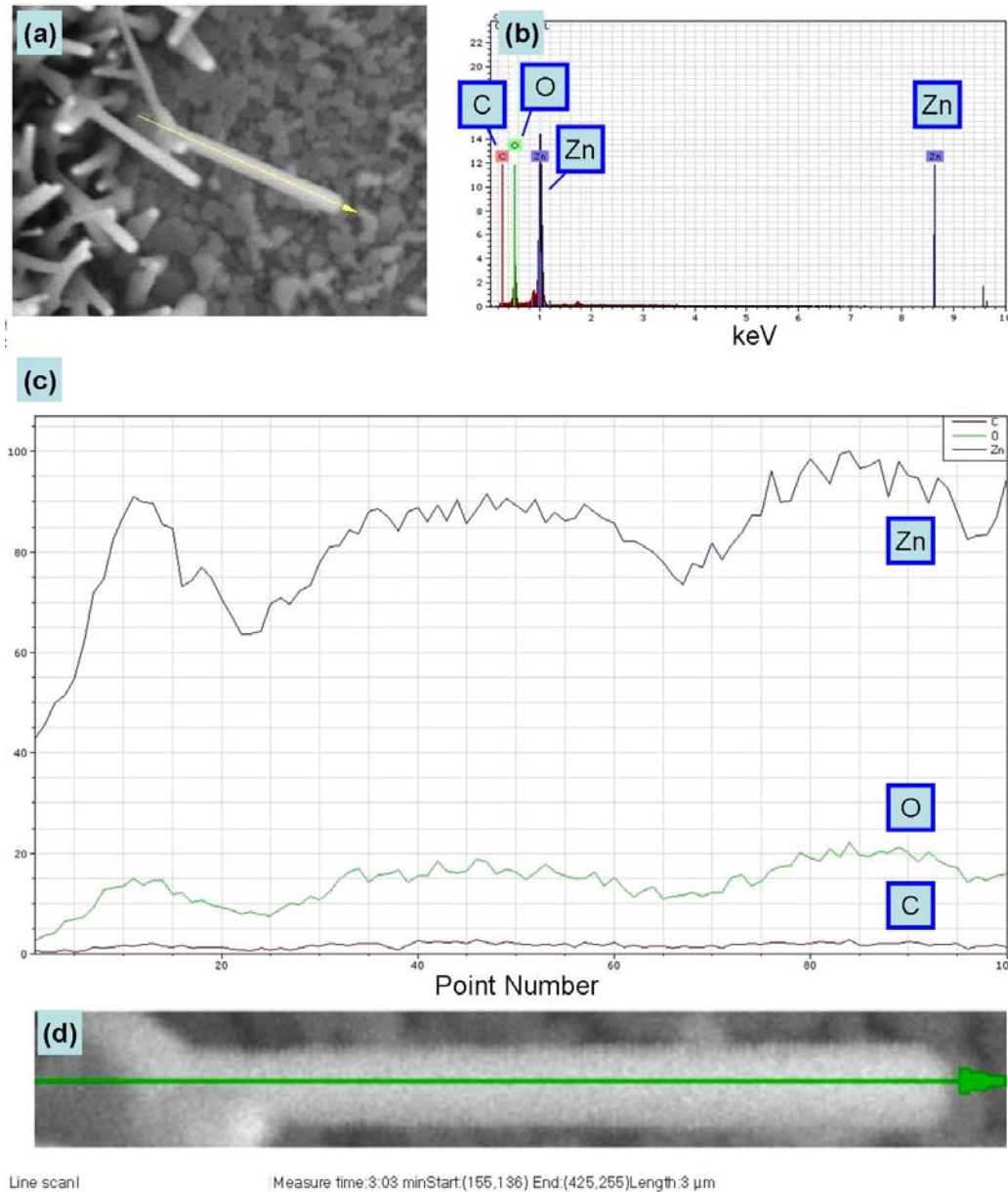


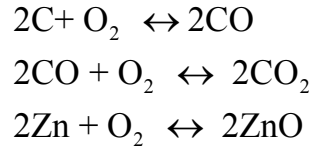
Figure 3.15 SEM image and EDS line scan. (a) is the SEM image of scanned area. The spectrum in (b) shows strong peaks of Zn, O and C (from the DLC film). The EDS line scan (c) reveals the ZnO NW is uniform with Zn and O exhibiting the same trend and C remains fairly constant and low. Image (d) is the 3 μm long single NW chosen to be examined for 3 mins from bottom to top.

3.3.2 Atomic Force Microscopy (AFM)

In order to understand the role of carbon in this growth process, we studied the interface between DLC film and the bottom of the ZnO NWs. Atomic force microscopy (AFM) was used for this investigation. After we fabricated the ZnO NWs on top of the DLC film, we put the sample into a 5% HCl (Hydrochloric acid) diluted solution for 24 hours. The diluted HCl solution etched out the ZnO NWs and selectively left the DLC film intact. The remaining DLC film on the substrate was analyzed by AFM to investigate the ZnO NWs/DLC interface (see [Figure 3.16](#)).

[Figure 3.16](#) (a) is the schematic (vertical and side view) of the SiO₂/Si substrate with 25 nm DLC pattern deposited by PLD at room temperature. Figure 3.16 (b) is the lower and higher magnification SEM images showing the ZnO NWs growth morphology on top of the DLC film. Figure 3.16 (c) is the AFM image of bare DLC film before NWs growth showing a fairly smooth surface. We also immersed the as deposited DLC film into the same 5% HCl solution for 24 hours to ensure that the DLC film has the resistance to the chemical solution. The “etched” DLC film showed a smooth surface still after etching.

The image in Figure 3.16 (d) is the surface topography of the sample with ZnO NWs grown after etching in a diluted HCl solution for 24 hours. The image shows a rough surface which suggests that some graphite (sp² bonding) portion of the DLC film was lost after undergoing a redox process near the substrate surface with the chemical reaction process suggested in reference [\[45\]](#). There are three reactions that involve oxygen in the carbon assisted thermal evaporation fabrication system:



Our results suggest that after growth of the ZnO NWs on the DLC film, some portion of carbon source (within the DLC film or at the DLC surface area) reacted with oxygen and became CO or CO₂ and was carried away by the carrier gas in the fabrication system. The C sublimation produced a rough surface of the DLC film that we observed after the diluted HCl solution etched away the ZnO NWs on the DLC film.

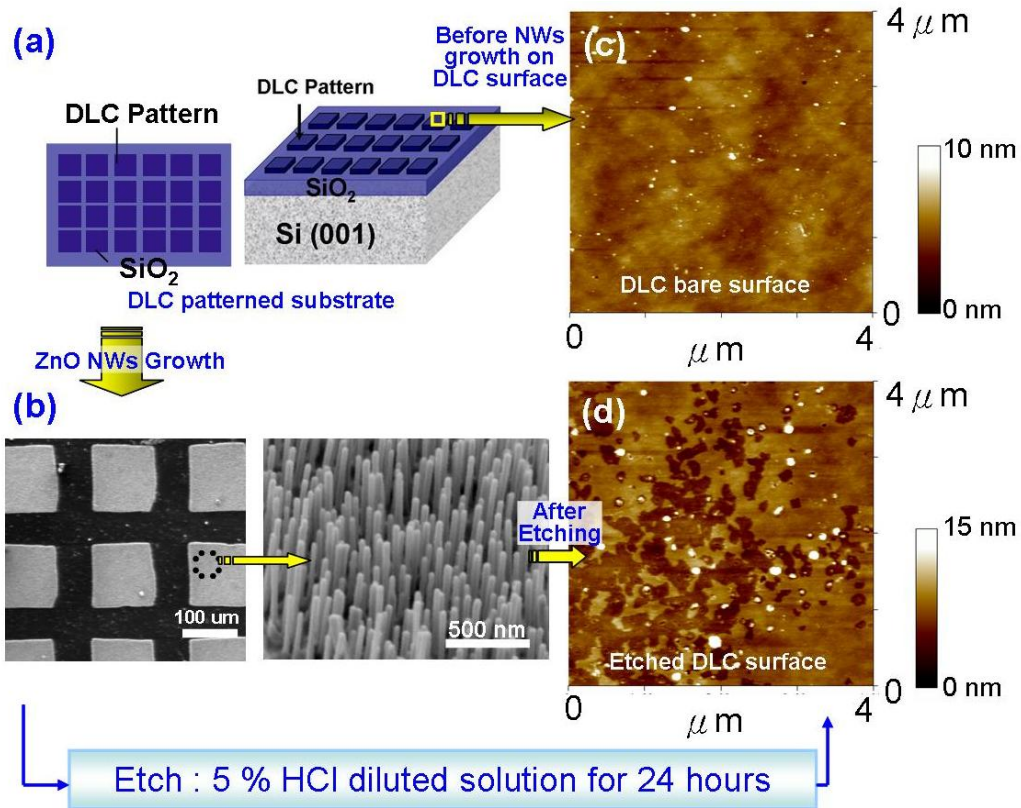


Figure 3.16 (a) is the schematic (vertical and side view) of Si (001) with 30 nm DLC pattern on top deposited at room temperature. (b) shows the SEM images after growth of ZnO NWs. AFM image (c) is the as deposited DLC film topography prior to NWs growth and (d) is the sample surface examined after etching in 5% HCl solution for 24 hours revealing the rough surface of the DLC after growth.

3.3.3 X-ray Diffraction (XRD)

Figure 3.17 is the comparison of X-ray Diffraction (XRD) spectra of (1) bare SiO₂/Si substrate, (2) DLC/SiO₂/Si, (3) ZnO NWs/DLC/SiO₂/Si growth and (4) after etching the NWs in diluted HCl solution for 24 hours.

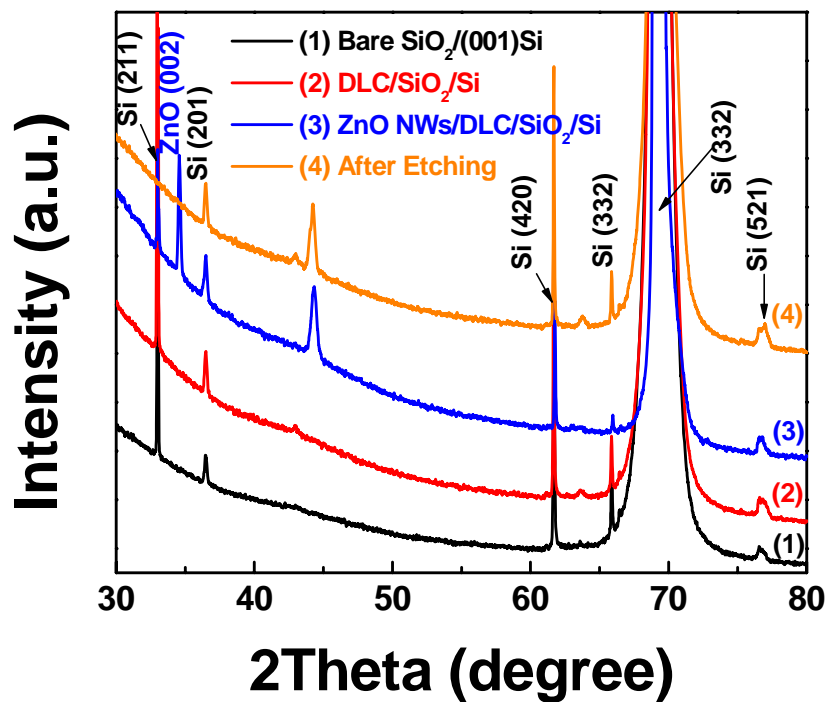


Figure 3.17 Comparison of X-ray Diffraction (XRD) spectra from bare SiO₂/Si substrate, DLC/SiO₂/Si, ZnO NWs/DLC/SiO₂/Si growth and after etching the NWs in diluted HCl solution for 24 hours. After etching (spectrum (4)), the ZnO NW (002) peak disappeared.

Among these XRD patterns, spectrum (2) shows that the as deposited DLC film is amorphous phase while the spectrum (3) shows a strong peak of ZnO (0002) at 34.5° and from the 2θ angle we can calculate the lattice parameter along the growth

direction c as $c_{ZnO\ NW} = 0.5195\ nm$. This value matches with the HRTEM result, see section 3.3.5 and agrees with the c -axis lattice constant reported for ZnO. The spectrum (4) shows that after etching with HCl solution, the (002) peak of ZnO is not present indicating that the NWs and any ZnO film under the NWs were etched from the DLC film surface. We examined the samples which gave rise to the spectra (3) and (4) with AFM scanning and the topography images are shown in Figures 3.16 (c) and (d), respectively.

3.3.4 Photoluminescence (PL)

Figure 3.17 compares photoluminescence spectra of ZnO NWs grown on DLC film and Au film on Si (001) substrates. The two spectra are almost identical except that the ZnO NWs' wavelength grown on Au is 1.5 nm longer. The difference is within the experimental error. The spectrum exhibits only a sharp intense UV emission peak around 380 nm (with 15 degree detection angle) which is attributed to the near band edge emission of ZnO. The band edge emission is due to a recombination of free-excitons through an exciton–exciton collision process. Note that the emission spectra can be recorded at different detection angles and consequently result in detecting various emission wavelengths from 387 nm ~ 380 nm [43]. The luminescence intensity dropped when the detection angle was increased (detecting angle started from 0° to 45°). This result indicates that the luminescence was emitted mainly along the axis of the ZnO nanorods. The luminescence peak shifted about 2 nm when the detection angle increased from 0 to 45 degrees. This may

also be caused by the polarization of the emitted light from the aligned nanorods. In addition, no broad defect-related green peak [11] is observed in the PL spectrum indicating good crystallinity of the ZnO material.

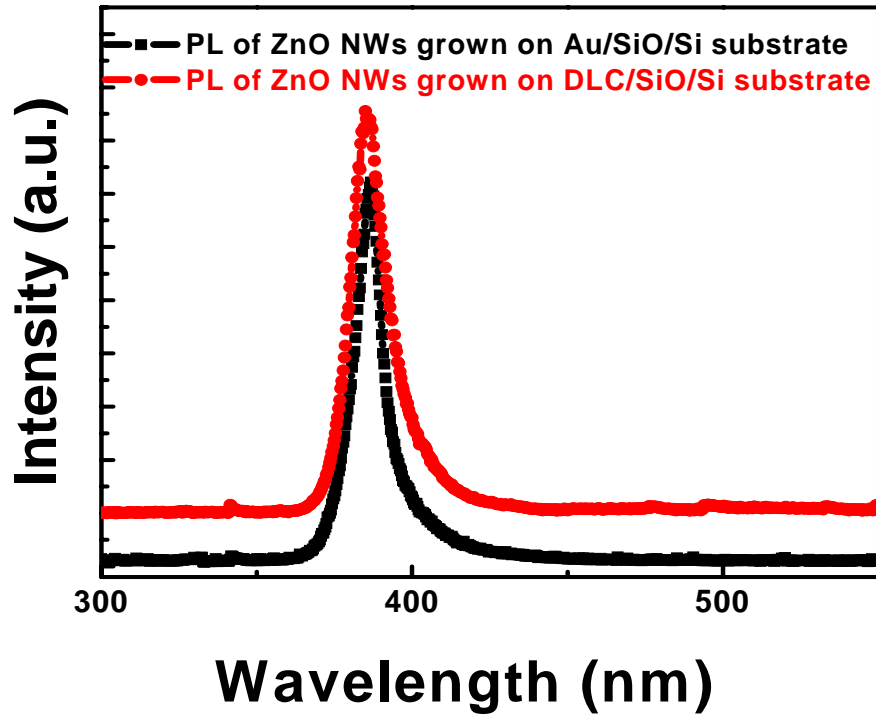


Figure 3.18 Photoluminescence (PL) spectra of ZnO NWs grown on DLC film (DLC/SiO₂/Si) and on Au film (Au/SiO₂/Si). The strong ultraviolet emission at around 380 nm is attributed to the near-band-edge emission of the wide bandgap ZnO.

3.3.5 Transmission electron microscopy (TEM)

In order to better understand the ZnO NWs' composition, nanostructure and growth mechanism, we carried out transmission electron microscopy (TEM) analysis of the ZnO NWs grown on DLC film. **Figures 3.19** (a) and (b) are cross-section and

top view SEM images of the ZnO NWs grown with the optimum conditions presented in section 3.2.4 (Figure 3.13). The diameter of the NWs ranges from 20 to 60 nm. (c) is the cross-section view TEM image and (d) and (e) are high-resolution TEM images from two different points along the nanowire. Both HRTEM images show single-crystal ZnO NW growth along [0001] direction with a c -lattice parameter of 0.5195 nm and $a = 0.3248$ nm indicating that the NW is single crystalline. Comparing the SEM images (a), (b) and the cross-section view TEM image (c), we can see that each NW grows on top of individual large ZnO grains with composition of ZnO slightly oxygen deficient as was confirmed by TEM-EDS and HRTEM examination. Therefore, the size of the grain determines the NWs' separation. We already discussed in section 3.2.1 that the DLC film deposition temperature is one of the most significant parameters affecting the ZnO grain size underneath the NWs. The ZnO grain size decreases with increasing deposition temperature. Therefore, the NW density is controllable.

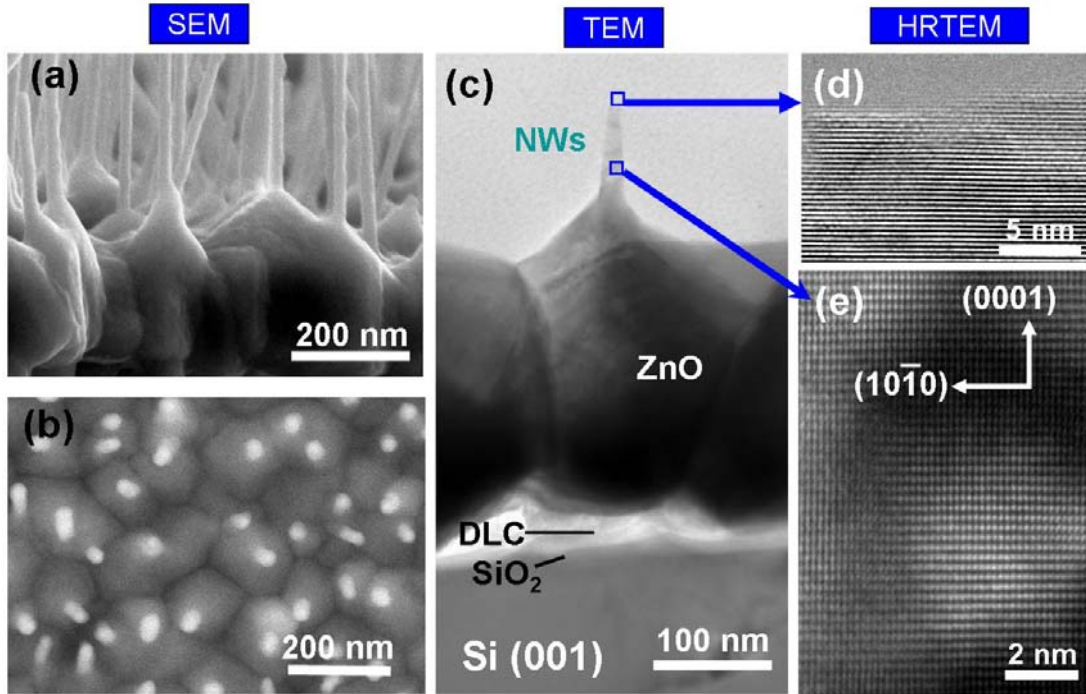


Figure 3.19 (a) and (b) are cross-section and top view SEM images of the ZnO NWs grown at optimum conditions for high density, thinner diameter and straight NWs on DLC film. The diameter of the NWs ranges from 20 to 80 nm. (c) is the cross-section view TEM image and (d), (e) are the high-resolution TEM images. (e) shows the nanostructure on the top part of the NW.

Figure 3.20 presents a TEM image that shows the area and directions along which EDS line scans were performed. Horizontal line scan (\square , red dash arrow) shows uniform composition and vertical line scan (∇ , blue dash arrow) shows the variation in the concentration of each element along the length of the NW. Note that the electron beam for EDS characterization may have broader contribution volume in the ZnO grain under the NW that gives rise to the variations in the concentration of each element in the vertical direction.

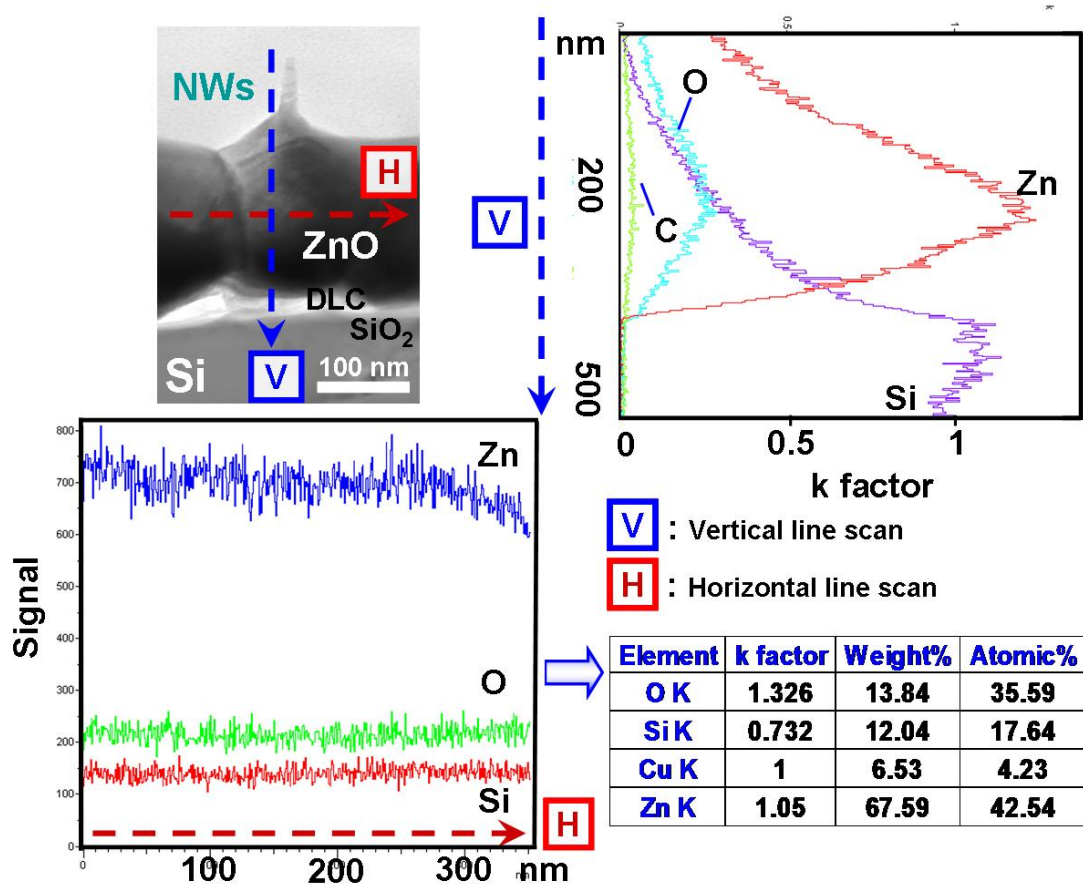


Figure 3.20 TEM image showing the area and directions along which EDS line scans were obtained. Horizontal line scan (H, red dash arrow) shows uniform composition and vertical line scan (V, blue dash arrow) shows the quantitative information of the concentration of each element. From the chart, we can see the ZnO NW is oxygen deficient. This results in the ZnO being an intrinsic n-type semiconductor.

To get more information about the composition of the NWs, we also utilized the TEM-EDS mapping analysis. **Figure 3.21** below shows the TEM image (a) with the selected area for EDS mapping. The TEM image shows the DLC film and SiO₂ layer underneath the ZnO grain/NWs. The images in Figure 3.21 (b) represent the elemental (Zn, O, C, and Si) maps of the selected area. Note that the M-bond epoxy used to prepare the TEM sample still remains over the top of the sample since the ion-milling process time after TEM sample polishing was short. From the images in

Figure 3.21 (b), we can see clear mapping of O, Zn, and Si since the ZnO grain/NWs and the Si substrate are well defined and show very strong contrast. The bright contrast underneath the ZnO grain in the O-map corresponds to the SiO₂ layer on top of the Si substrate. There is C present not only in the DLC film area, but also in the ZnO grains under the NWs which implies a slight C content incorporation in the ZnO at the beginning of the growth. This result also agrees with our model for the growth of ZnO on DLC by direct participation of the sp² bonding portion of the DLC in the ZnO NWs growth evolution with carbonic redox processes. Interestingly, the C-map shows very little C content (low k-factor) in the ZnO NWs area. Note that relatively strong contrast of C element in the EDS map is observed on top of the ZnO NWs, which originates from the M-bond epoxy.

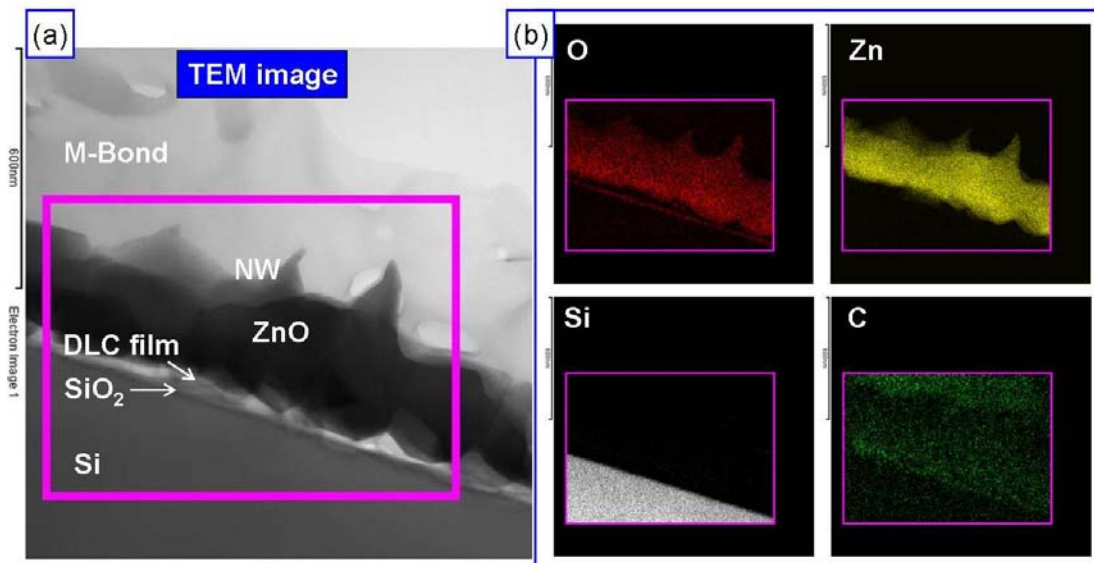


Figure 3.21 TEM image (a) shows the selected area for EDS mapping. Note that the M-bond still exist over the NWs since the ion-milling time for TEM sample preparation was short. The EDS maps in (b) are for O, Zn, C and Si.

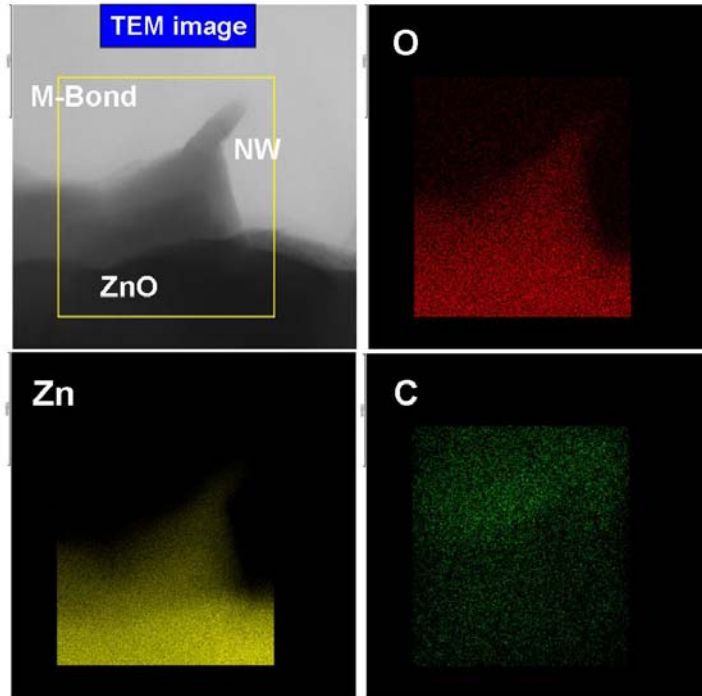


Figure 3.22 TEM image and EDS maps from a single ZnO NW area. The elemental maps show that the NW is pure ZnO and there is no C content within it.

TEM-EDS mapping from a single ZnO NW is shown in **Figure 3.22**. We examined only the ZnO area and obtained the same result for the concentration as in Figure 3.21. The elemental maps for Zn and O show uniform concentration at the ZnO grain/NW area and there is no C content in the NWs which also demonstrates that the C (graphite) help to improve the growth during first stage of growth and then the composition turns to pure ZnO during the growth of the nanowires on top.

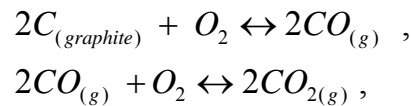
3.4 ZnO NWs Growth Mechanism

For both, the scientific understanding and potential applications of ZnO NWs it is necessary to understand and control the growth mechanism. In this research, we

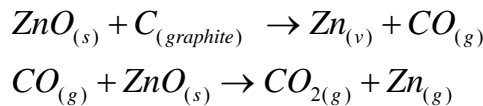
obtained the growth conditions to fabricate dense, uniform, vertically aligned ZnO NWs on DLC film pre-deposited on Si (001) substrates. The questions now are: How do the NWs grow? Why the DLC film helps during the ZnO NW growth process? What is the role of DLC on the growth of the nanowires? And what is the effect of the DLC on the properties of the NWs?

According to our experiments, we can control the NWs' length, diameter, density and orientation by varying the DLC film growth condition (see section 3.2). It's a well known and a common deposition tendency that increasing the DLC deposition temperature results in lower sp^2/sp^3 bonding ratio in the DLC film [36-38]. The dependence of sp^2/sp^3 bonding ratio in DLC on temperature showed an effect on the ZnO NWs growth mechanism in our study; i.e. high deposition temperature of the DLC film leads to longer ZnO NWs in our growth system. This also introduces significant chemical reactions among Zn, C, ZnO and CO_2 [44, 45].

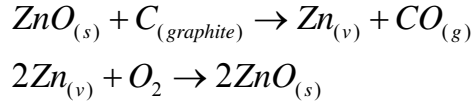
Our results are consistent with the following chemical reactions near the DLC film surface during growth of the NWs. First:



As the temperature is increased to the reaction temperature, the ZnO is reduced by $C_{(graphite)}$ and $CO_{(g)}$. The reactions can be described as follows:



When the Zn or ZnO vapor arrives at the surface of the substrate, the chemical reaction may be expressed as follows:

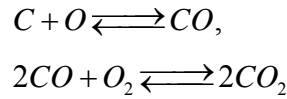


Most of the research on ZnO NW fabrication involving graphite, is carried out using ZnO powder mixed with about 20~ 50 wt% of graphite powder as the source material. However, the mechanism for the growth of the NWs is not clear at the present time. In our research, the carbon resource solely came from the DLC film. The CO_x enriched in the vicinity of the DLC film served as the only carbon source (**Figure 3.23**). The melting point of pure Zn is 419.58 °C and the boiling point is about 907 °C. From our experiments, the best growth temperature for the growth of ZnO NWs on the DLC film (not Au film) was usually higher than 900 °C (for Au film assisted, the growth temperature can be lower). Thus, the Zn powder will be evaporated as vapor phase and transported downstream via the carrier gas (Ar/O₂). When Zn_(v) is being transported, it reacts with oxygen gas and become ZnO_(v,l) ($2\text{Zn} + \text{O}_2 \rightarrow 2\text{ZnO}$) before arriving at the substrate. However, we can also expect that some pure Zn_(v) will arrive at the substrate. This Zn could also react with the C in the DLC to form ZnO as shown above.

It's known that ZnO and C are immiscible. When the DLC film surface is full of carbon atoms and Zn atoms impinge on the DLC surface, the immiscibility between ZnO and C will act as a driving force and impel the ZnO cluster toward the point of lower free energy [46]. This impelling force is insufficient when the ZnO clusters become too large. This may explain why the DLC film deposition temperature can change the ZnO grains underneath the NWs. When the DLC film deposition temperature is higher, the C_(sp² bonding) of the DLC film decreases. The impelling force

on the ZnO clusters/nuclei is lower and the mobility of the nuclei is also lower. That is, when the $Zn_{(v)}$ drop to the DLC film surface, most of the drops may stay where they dropped since there is insufficient driving force to impel them toward the lower free energy area. Consequently, the first stage of growth is the formation of small ZnO grains (before ZnO NWs formation). The growth of ZnO grains is three dimensional; the horizontal direction will cease when the grains meet each other. Once the ZnO grains have formed, nanowires begin to grow along the [0001] preferred direction.

In addition, the vicinity of DLC film is CO_x enriched as follow [45],



The carbon, $C_{(sp^2 \text{ bonding})}$, at the surface of the DLC may have the reaction, $ZnO_{(s,l)} + C_{(s)} \rightleftharpoons Zn_{(v)} + CO_{(v)}$. According to Ellingham diagram, the reaction above takes place when the temperature is higher than 970 °C; however, in the surface region, the reduction of ZnO reaction might be possible when the temperature is lower than that and the oxygen partial pressure is low. These chain of reactions gives rise to ZnO grains underneath the NWs. Note that defects and grain boundaries in the ZnO grains are expected to exist and provide an easy diffusion path for the CO/CO₂ gas phase [47]. This could explain why the carbon element was found within the ZnO grains/films in our TEM-EDS characterization.

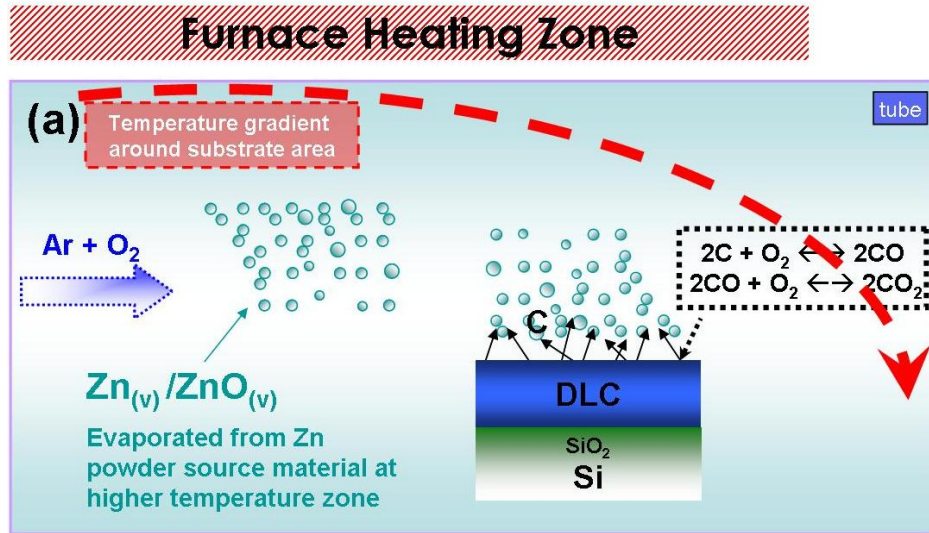
Since the DLC film is the only carbon source in our experiments and the carbon content participates in the chemical reaction near the DLC film surface area; it demonstrates why this layer becomes rough after the growth of the NWs as we found

in our AFM images after etching the NWs (Figure 3.16) that DLC film had holes after carbonic reactions. We can also see some of the voids in the DLC film surface from our TEM images (Figure 3.18 (c)). These investigations provide additional evidence for how the carbon participates in the ZnO NWs growth.

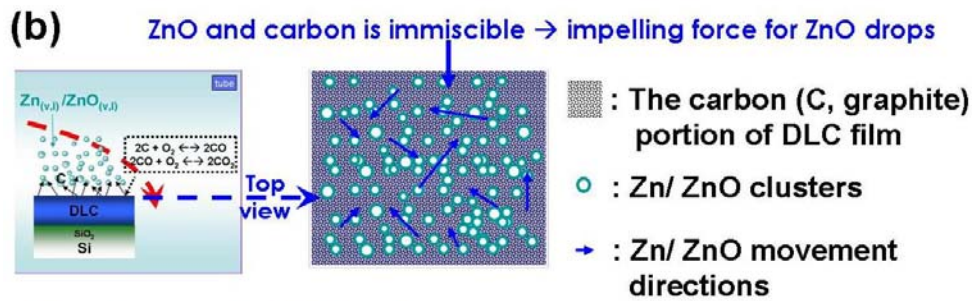
After the 3D growth of the ZnO grains towards the $(0001)/(000\bar{1})$ and also the side directions $\{10\bar{1}0\}$, the NWs begin to grow on the ZnO grains. It is important to note that the $(0001)/(000\bar{1})$ surfaces have the lowest Gibbs free energy in ZnO. The Gibbs free energy difference ($\Delta G_s = \Delta G_{s_{3D}} - \Delta G_{s_{1D}}$) > 0 when the dimension changes from 3D to 1D for a hexagonal nucleus with the same height and side length (a) as given by [46],

$$\Delta G_s = 13.92a \left(\sqrt{\left(\frac{2}{3\sqrt{3}a}\right) + a^2} \right) - a + \frac{2.7714}{a} > 0 ; \text{ for 1D preferred growth.}$$

Therefore, in order to minimize the Gibbs free energy of the ZnO NWs nucleus, the one dimensional growth is thermodynamically favorable. From this, we can explain the ZnO NWs' morphologies we fabricated in our experiments as schematically shown in Figure 3.14 (a ~ d).



Furnace Heating Zone



Reactions on the DLC surface area :

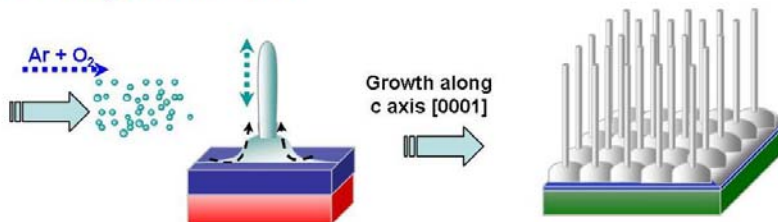
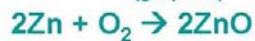


Figure 3.23 (a) Schematic of the evaporation of Zn, chemical vapor, transport and condensation during fabrication process. Zn evaporates from the Zn metal powder from higher temperature zone located upstream and transported by the carrier gas (Ar/O₂) to the surface of DLC film and reacts with C and O. (b) Vertical view schematic of the DLC film surface. The arrows show the movements of ZnO impelled by the driving force resulting from its immiscibility with C on the surface. It also shows the possible reactions between ZnO and C at the DLC surface and the morphology of the ZnO NWs.

Chapter 4

Summary and Suggestions for Future Work

4.1 Summary

In this thesis, ZnO NWs grown on top of DLC film were fabricated and the dependences of the diameter, density and length of the NWs on the growth parameters were studied. We first fabricated the NWs with the assistance of predeposited Au thin film on Si (001) substrates, in order to obtain the optimum growth condition for our fabrication system.

DLC films have not only outstanding optical properties, but also provide an excellent material for the understanding of the ZnO NWs growth mechanism. The combination and architecture of ZnO NWs and DLC films could be a phenomenal material for a wide variety of optoelectronic applications.

In this research, we successfully fabricated dense, uniform and vertically aligned ZnO NWs on DLC films pre-coated on Si (001) substrates without the use of any metal catalyst. The morphology of the ZnO NWs has a strong dependence on growth parameters. In most of the experimental results, a ZnO polycrystalline layer forms first. From this layer ZnO NWs grow on top of it. The NWs portion has two sections. The bottom section has wider diameter that varies from 100 nm up to 1 μm , depending on the growth conditions. The thinner section on top uniformly grows

down to ~ 20 nm in diameter and has a c -axis orientation along the growth direction. The NWs extend for $3 \sim 5 \mu\text{m}$ in length.

Our results reveal the growth dependence on the deposition temperature of the DLC film. It is known that the DLC films deposited by plasma deposition show lower sp^2/sp^3 bonding ratio at higher deposition temperatures. Our results show that the ZnO NWs grow longer on top of the DLC film deposited at lower temperature. The carbon content in the DLC film plays an important role in the growth process.

In order to characterize the NWs, several techniques were used. From SEM examination, we can directly see the morphology of the as fabricated ZnO NWs. XRD analysis showed that the NWs' have c -axis orientation with lattice parameter, $c = 0.5195$ nm. Furthermore, we checked the nanostructure utilizing TEM to confirm the ZnO NWs and found that they are single crystalline. The interface area was also investigated by EDS in SEM and TEM to obtain elemental maps and discovered the dispersion and reaction of the carbon content during the growth process. Combining these results with the AFM topography results, we established a model for the growth mechanism for DLC assisted ZnO NW growth.

4.2 Suggestions for Future Work

DLC thin film has attracted tremendous attention because of its field emission applications. The advantages of carbon cathode include: (i) chemical and physical stability; (ii) more resistant to poisoning by foreign elements; (iii) low sputter yield

(when bombarded by residual ions in the device); (iv) low cost for deposition and (v) it can almost be deposited on any surface. However, the disadvantages of it are (i) low emission site density (ESD); (ii) relatively low maximum current density.

These properties may improve by the deposition of ZnO NWs on top of DLC to significantly enhance the field emission properties. G.W. Yang et al. [45] studied the field emission properties of ZnO NWs grown on amorphous diamond. A remarkable field emission enhancement by the ZnO nanowires covered amorphous diamond nanocomposite was observed, suggesting that the combined effect of the field emission of ZnO nanowires and amorphous diamond has potential for applications in displays and other areas. However, up to now, it has been difficult to fabricate well aligned vertically grown ZnO NWs.

For the future work, we can focus on a more detailed study of the control of the morphology by the DLC film. Build a more detailed growth condition map showing the optimized growth parameters, since for different applications and usages, different ZnO NWs' morphology/shape, diameter and separation distance may be required. It is also important to investigate the field emission property and breakdown voltage of the fabricated ZnO NWs developed in this research.

Furthermore, we were able to obtain very sharp (~5nm in diameter tip) ZnO NWs at higher oxygen partial pressure. The ultra thin NWs were seen but not all over the sample. However, since this dimension is very promising for nanodevice applications, we should fine tune the fabrication parameters to find out what is the optimum growth condition to uniformly fabricate these ultra thin ZnO NWs. In addition, it is also important to investigate their field emission properties.

References:

1. Y. Sun, M. N R Ashfold, *Nanotechnology* **18** (2007), 245701
2. S. Iijima, *Nature* **354** (1991) 56–8.
3. Z. K. Tang, G. L. Wong, P. Yu, M. Kawasaki, A. Ohtomo, H. Koinuma, Y. Segawa, *Appl. Phys. Lett.* **72** (1998), 3270
4. D. M. Bagnall, Y. F. Chen, Z. Zhu, T. Yao, S. Koyama, M.Y. Shen and T. Goto, *Appl. Phys. Lett.* **70** (1997), 2230
5. B.S. Zou, R.B. Liu, F.F. Wang, A.L. Pan, L. Cao and Z. L. Wang, *J. Phys. Chem. B* **110** (2006), 12865
6. A. Osinsky, J.W. Dong, M.Z. Kauser, B. Hertog, A.M. Dabrian, P.P. Chow, S.J. Pearton, O. Lopatiuk and L. Chernyak, *Appl. Phys. Lett.* **85** (2004), 4272
7. J.F. Wager, *Science*, **300** (2003), 1245
8. Aoki T., Hatanaka Y. and Look D. C., *Appl. Phys. Lett.* **76** (2000), 3257
9. Y.Xia, P. Yang, Y. Sun, Y. Wu, B. Mayer, B. Gates, Y. Yin, F. Kim, H. Yan, *Adv. Mater.*, **15** (2003), 353
10. H. Kind, H. Yang, M. Law, B. Messer, P. Yang, *Adv. Mater.*, **14** (2002), 158
11. Y.W. Heo, D.P. Norton, L.C. Tien, Y. Kwon, B.S. Kang, F. Ren, S.J. Pearton and J.R. LaRoche, *Mater. Sci. Eng. R* **47** (2004), 1
12. Z.L. Wang, X.Y. Kong, Y. Ding, P.X. Gao, W.L. Hughes, R. Yang, Y. Zhang, *Adv. Funct. Mater.* **14** (2004), 943
13. Z. W. Pang, Z. R. Dai, and Z. L. Wang, *Science*, **291** (2001), 1947
14. X. Y. Kong, Y. D., R. Yang, and Z. L. Wang, *Science*, **303** (2004), 1348
15. J. Y. Lao, J. Y. Huang, and Z. F. Ren, *Nano Lett.*, **3** (2003), 235
16. M. H. Huang, Y. Wu, H. Feick, N. Tran, E. Weber, P. Yang, *Adv. Mater.*, **13** (2001), 113
17. Park W. I., Yi G. C., Kim M. and Pennycook S. J., *Adv. Mater.* **14** (2002), 1841
18. Okada T., Agung B. H. and Nakata Y., *Appl. Phys. A* **79** (2004), 1417
19. Liu X., Wu X., Cao H. and Chang R. P. H., *J. Appl. Phys.* **95** (2004), 3141
20. Huang M. H., Mao S., Feick H., Yan H., Wu Y., Kind H., Weber E., Russo R. and Yang P. D., *Science* **292** (2001), 1897
21. Ng H. T., Li J., Smith M. K., Nguyen P., Cassell A., Han J. and Meyyappan M., *Science* **300** (2003), 1249
22. Lao J. Y., Wen J. G. and Ren Z. F., *Nano Lett.* **2** (2002), 1287
23. Lao C. S., Gao P. X., Yang R. S., Zhang Y., Dai Y. and Wang Z. L., *Chem. Phys. Lett.* **417** (2006), 358
24. E. Comini, G. Faglia, G. Sberveglieri, Z. W. Pan and Z. L. Wang, *Appl. Phys. Lett.* **81** (2002), 1869
25. X. D. Bai, P. X. Gao, Z. L. Wang and E. G. Wang, *Appl. Phys. Lett.* **82** (2003), 4806
26. W. Hughes and Z. L. Wang, *Appl. Phys. Lett.* **82** (2003), 2886
27. Gao P. X., Ding Y. and Wang Z. L., *Nano Lett.* **3** (2003), 1315
28. Greyson E. C., Babayan Y. and Odom T. W., *Adv. Mater.* **16** (2004), 1348

29. Choy J. H., Jang E. S., Won J. H., Chung J. H., Jang D. J. and Kim Y.W., *Adv. Mater.* **15** (2003), 1911
30. Yamabi S. and Imai H., *J. Mater. Chem.* **12** (2002), 3773
31. L. E. Greene, M. Law, D. H. Tan, M. Montano, J. Goldberger, G. Somorjai, and P. D. Yang, *Nano Lett.* **5** (2005), 1231
32. S. H. Dalal, D. L. Baptista, K. B.K. Teo, R. G. Lacerda, D. A. Jefferson and W. I. Milne, *Nanotechnology* **17** (2006), 4811
33. Koh Y. W., Lin M., Tan C. K., Foo Y. L. and Loh K. P., *J. Phys. Chem. B*, **108** (2004), 11419
34. Bae S. Y., Seo H. W., Choi H. C. and Park J., *J. Phys. Chem. B* **108** (2004), 12318
35. W. -D. Zhang, *Nanotechnology* **17** (2006), 1036
36. J. Robertson, *Mater. Sci. Eng. R* **37** (2002), 129
37. M. P. Siegal, D. R. Tallant, P. N. Provencio, D. L. Overmyer, and R. L. Simpson, L. J. Martinez-Miranda, *Appl. Phys. Lett.* **76** (2000), 3052
38. L. J. Martinez-Miranda, M. P. Siegal and P. P. Provencio, *Appl. Phys. Lett.* **79** (2001), 542
39. Y. H. Yang, C.X. Wang, B. Wang, N.S. Xu, G.W. Yang, *Chem. Phys. Lett.* **403** (2005), 248; superconductivity.et.anl.gov/Techniques/PLD
40. D. McQuarrie, J. Simon, *Physical Chemistry: A Molecular Approach*, University Science Books, 1997
41. C. J. Lee, T. J. Lee, S. C. Lyu, Y. Zhang. H. Ruh, H. J. Lee, *Appl. Phys. Lett.* **81** (2002), 2886
42. S. H. Jo, J. Y. Lao, Z. F. Ren, R. A. Farre, T. Baldacchini, J. T. Fourkas, *Appl. Phys. Lett.* **83** (2004), 4821
43. X. Wang, C. J. Smuwers, Z. L. Wang, *Nano Lett.* **3** (2004), 423
44. S. Y. Li, P. Lin, C. Y. Lee, T. Y. Tseng, *J. Appl. Phys.* **95** (2004), 3711
45. J. Song, X. Wang, E. Riedo, Z. L Wang, *J. Phys. Chem. Lett. B* **109** (2005), 9869
46. Y. H. Yang, B. Wang, G.W. Yang, *Cryst. Growth Des.* **7** (2007) 1242
47. Q Li, K. W. Kwong, *Phys. Rev. Lett.* **92** (2004) 186102